

# Structure and Evolution of Low-Mass Stars: An Overview and Some Open Problems

M. Catelan

*Pontificia Universidad Católica de Chile, Departamento de Astronomía y Astrofísica,  
Av. Vicuña Mackenna 4860, 782-0436 Macul, Santiago, Chile  
e-mail: mcatelan@astro.puc.cl*

**Abstract.** A review is presented of some of the ingredients, assumptions and techniques that are used in the computation of the structure and evolution of low-mass stars. Emphasis is placed on several ingredients which are still subject to considerable uncertainty. An overview of the evolution of low-mass stars is also presented, from the cloud collapse phase all the way to the white dwarf cooling curve.

**Keywords:** stars: interiors; stars: low-mass; stars: evolution; stars: general; stars: Hertzsprung-Russell diagram

**PACS:** 95.30.-k; 95.30.Tg; 97.10.Cv; 97.10.Zr

## 1. DEFINITION OF “LOW-MASS STARS”

Low-mass stars are self-gravitating gaseous (or, rather, plasmatic) bodies that develop electron-degenerate cores (meaning that all low-lying energy states are filled and electron pressure is accordingly dominated by the Pauli exclusion principle) soon after leaving the main sequence (MS) phase, and hence undergo the so-called “helium flash” (i.e., ignition of the triple- $\alpha$  process, whereby three alpha particles are converted into a  $^{12}\text{C}$  nucleus, under degenerate conditions) at the end of their evolution on the red giant branch (RGB). Evolutionary calculations indicate that this corresponds to an upper mass limit  $M \approx 2 - 2.5 M_{\odot}$  (e.g., [258, 259, 109]). Exceptionally, and as a consequence of extreme mass loss on the RGB, some such stars may directly become helium white dwarfs (WD’s) before they are ever able to ignite helium in their degenerate cores (e.g., [16] and references therein). At the low-mass end, on the other hand, one finds that objects below  $M \simeq 0.08 M_{\odot}$  are incapable of quiescent hydrogen burning. This corresponds to the commonly adopted “dividing line” between low-mass stars and the so-called brown dwarfs (see, e.g., [58], and references therein). Empirically, the latter have recently been associated to the new spectral classes L ([156]) and T ([31]).

## 2. ASTROPHYSICAL IMPORTANCE

Low-mass stars are of great astrophysical importance for a variety of reasons, which include the following:

- Due to the shape of the so-called “Initial Mass Function” ([227]; see also [163] for a recent review), which gives the number of stars that are born in a given

population as a function of mass, most stars in the Universe are low-mass stars. As a consequence, and in spite of their lower individual masses, most of the baryonic mass in the Universe currently in the form of stars is also contained in low-mass stars (and their remnants), even though, to be sure, most baryonic mass actually appears to be in the form of gas ([102]). Most importantly, low-mass stars dominate the integrated light in old stellar systems, including elliptical galaxies and the spheroids (bulges and halos) of spiral galaxies. Therefore, in a very real sense, it is not possible to understand the properties of distant galaxies without adequate models of low-mass structure and evolution.

- In the same token, (bona-fide) globular star clusters are almost exclusively comprised of low-mass stars. Given that resolved Galactic globular clusters have long been known ([229]) to be the oldest objects in the Universe for which reliable ages can be determined, they play a crucial cosmological role, since the oldest stars in the Universe cannot be older than the Universe itself (see, e.g., [110, 157, 158, 159, 100]). The latter, according to the latest results from the WMAP experiment [248, 249], is  $13.73^{+0.13}_{-0.17}$  Gyr old. Cluster ages are determined by comparison of the observed color-magnitude diagrams of globular clusters with theoretical isochrones,<sup>1</sup> especially around the so-called “turn-off point” (see §5) – which occurs as a consequence of hydrogen exhaustion in the core (see, e.g., [172] for a recent discussion). Recent age determinations for the oldest, most metal-poor Galactic globular clusters (such as M92 = NGC 6341) include those by [273] (13.5 Gyr), who also revise downward (by incorporating diffusion in their models) the age obtained, using high-quality Strömgren photometry and a distance-independent method, by [117], which was clearly much higher than the age of the Universe favored by WMAP; and those by [230] (in the 12–14 Gyr range). While these ages appear broadly consistent with the favored WMAP age, it should be noted that the recently suggested revision in the abundances of elements in the Sun, based on 3D models of the solar convective region (e.g., [2, 6, 5]), will lead, according to [189], to an *upward* change (by  $\approx 0.7$  Gyr) in the cluster ages, which may complicate the agreement between WMAP and globular cluster results, especially (e.g., [57]) when the formation and chemical evolution time before the oldest globular clusters were born is properly accounted for. The latter time interval, according to [160], is likely to be in the 0.3 – 3 Gyr range. On the other hand, another recent study ([81]) concludes instead that the new abundances will indeed lead to an increase in cluster ages (by a maximum of  $\sim 10\%$ ), but only for *open* clusters, globular cluster ages remaining instead essentially unchanged with respect to previous models.
- Low-mass stars can be used as a probe of the properties of fundamental particles that are already present within the so-called Standard Model of particle physics, as well as on the existence and nature of (non-standard) dark matter particle candidates

---

<sup>1</sup> An isochrone – from the greek *iso* = same, *chronos* = age – represents the geometric locus occupied by stars of a given chemical composition that are born with different masses. Seemingly, the first “modern” isochrones were computed by [83]. A nice qualitative description of how isochrones are built is provided in [140], whereas more quantitative details can be found, for instance, in [17].

(e.g., [197, 199] and references therein). For instance, the cooling of low-mass RGB stars would be affected by a non-zero neutrino magnetic moment, thereby impacting such important observables as the magnitude of the RGB tip, the absolute magnitude of the horizontal branch (HB), the pulsation periods of RR Lyrae stars, and the relative proportion of stars on the RGB, HB, and asymptotic giant branch (AGB). By comparing theoretical models in which a neutrino magnetic moment is included with the observations, one obtains a very stringent bound on this quantity ([196, 204, 56]), which in fact is several orders of magnitude more stringent than is possible to achieve at present from laboratory experiments (e.g., [198] and references therein). Using similar arguments, stringent limits can also be placed on the electric charge of the neutrino ([198]), the mass and other interaction properties of the axion (e.g., [203, 56, 200, 201, 202]), and even the size of large extra dimensions ([45]) – though in the latter case more stringent constraints can be obtained from WD’s ([20]) and (especially) neutron stars ([122]).

- Finally, it is also worth recalling that our own existence crucially depends on the properties of a low-mass star (the Sun), whose past and future evolution are accordingly crucial in determining our origin and destiny in the Universe. For instance, the Earth may or may not, depending on the amount of mass lost in the form of stellar winds (which unfortunately we are unable to predict from first principles at present) during its evolution as a red giant, be completely engulfed by the Sun during the latter’s evolution as an AGB star, when its age is around 12 – 12.5 Gyr ([222]). The reason is that, while it is clear that the solar radius will expand enormously during its evolution as a red giant, the actual orbital radii of the planets will move out as a consequence of mass loss from the Sun, the ultimate fate of the Earth and the other inner planets depending on how much mass exactly is lost during the Sun’s evolution as a red giant. In fact, the Earth’s oceans will likely evaporate and its atmosphere be lost to space even before the Sun reaches the turnoff point, when its luminosity becomes 10% of more higher than its present value (see [205, 118] for reviews and additional references).

### 3. THE “STANDARD” OR “CANONICAL” THEORY OF STELLAR STRUCTURE AND EVOLUTION

While the theory of stellar structure and evolution is one of the oldest and most successful of all astrophysical theories, it is still subject to a number of approximations and limitations which often make their predictive power less optimum than is commonly realized. In the following sections, an overview is provided of the main ingredients that enter stellar structure/evolution calculations for low-mass stars, highlighting some of the current limitations and problems encountered when comparing models and observations.

As an editorial remark, the reader who may be interested in an overview of the evolution of low-mass stars before digging into a mathematical discussion of the principles of stellar structure and evolution is encouraged to proceed directly to §5, later returning to §3.1 in order to better appreciate the techniques that are used to arrive at some of the results discussed in §5.

### 3.1. The Four Basic Equations of Stellar Structure/Evolution

The modern phase of stellar structure/evolution studies was born with the advent of nuclear astrophysics, when the role of thermonuclear reactions in stellar interiors became clear ([18, 19, 105]). The roughly 70 years since this major development have been mostly devoted to refining the physical ingredients that enter the same basic set of four differential equations already known at that time, namely:

$$\frac{\partial r}{\partial m} = \frac{1}{4\pi r^2 \rho}, \quad (1)$$

$$\frac{\partial P}{\partial m} = -\frac{Gm}{4\pi r^4}, \quad (2)$$

$$\frac{\partial L}{\partial m} = \varepsilon - \varepsilon_v - \varepsilon_g, \quad (3)$$

$$\frac{\partial T}{\partial m} = -\frac{GmT}{4\pi r^4 P} \nabla, \quad (4)$$

where

$$\nabla \equiv \frac{\partial \ln T}{\partial \ln P}. \quad (5)$$

Here,  $r$  is the distance from the star center, and  $m$  is the mass contained within this distance.  $P$ ,  $\rho$ , and  $T$  are the thermodynamic variables pressure, density, and temperature, respectively, while  $L$  is the luminosity (in units of energy per unit time) at the position corresponding to  $m$  (or  $r$ ). (When  $r$  is used as the independent variable, one is talking about the *Eulerian formalism*, whereas  $m$  is used as independent variable – as above – in the so-called *Lagrangian formalism*.) Finally,  $\varepsilon$  corresponds to the energy generation rate (in the form of thermonuclear reactions),  $\varepsilon_v$  to the energy loss rate (in the form of neutrinos), and  $\varepsilon_g$  to the work that is performed on the gas (per unit time per unit mass) during any expansion/contraction of the star (for an ideal gas, it can easily be shown that  $\varepsilon_g = TdS/dt$ , where  $S$  is the specific entropy).  $G$ , as usual, is the Newtonian constant of gravitation. Note that partial derivatives have been used throughout to emphasize that the physical solutions that satisfy these equations are not stationary, but rather evolve with time, as a consequence of the nuclear transmutations in the stellar interior and the ensuing changes in chemical composition and mean molecular weight  $\mu$  brought about by the thermonuclear reactions.

Each one of these basic equations is extensively discussed in any stellar structure/evolution textbook (e.g., [234, 71, 76, 123, 223]), so that we will not go through their derivation in detail. These equations are, in the order they appear, the *mass conservation equation*, the *hydrostatic equilibrium equation*, the *energy conservation equation*, and the *energy transport equation*. While the first two are of chief importance in determining the mass profile inside the star (and are in fact the only ones used in the theory of self-gravitating, “polytropic” gas spheres; see, e.g., [96, 59]), the latter two are of paramount importance in defining the *thermal profile* of the star. Naturally, the latter

can only be accomplished with a theory of energy transport inside the star, which must somehow appear in relation with eq. (4). We will come back to this point later.

### 3.2. The Constitutive Equations

What the reader should realize at this point is that, even though we have a system of four equations, we actually have five unknown quantities that appear explicitly in them, namely:  $r$ ,  $\rho$ ,  $P$ ,  $L$ ,  $T$ . Therefore, in order to be able to solve the system, we need one additional equation. This is given by the *equation of state* (EOS), which provides one of the thermodynamic quantities in terms of the others; for instance,  $\rho = \rho(P, T, \mu)$ . The reader is referred to the Appendix in [274] for a discussion of and references to the different EOS implementations commonly adopted in low-mass stellar interiors work.<sup>2</sup>

As such, the EOS is often called one of the *constitutive equations* of stellar structure/evolution, describing as it does a physical property of the matter in the stellar interior. The perceptive reader will have noticed that additional constitutive equations are still needed in order to solve the problem, since several additional quantities (such as the  $\varepsilon$ 's) also enter these equations. Within this framework, the complete set of constitutive equations can be written as follows:

$$\rho = \rho(P, T, \mu), \quad (6)$$

$$c_P = c_P(P, T, \mu), \quad (7)$$

$$\kappa_v = \kappa_v(P, T, \mu), \quad (8)$$

$$r_{jk} = r_{jk}(P, T, \mu), \quad (9)$$

$$\varepsilon_v = \varepsilon_v(P, T, \mu), \quad (10)$$

where  $c_P$  is the specific heat at constant pressure,  $\kappa_v$  is the monochromatic opacity, and  $r_{jk}$  is the thermonuclear reaction rate for reactions that transform nuclei of type  $j$  into nuclei of type  $k$  (the corresponding energy generation rate  $\varepsilon_{jk}$  being given by  $Q_{jk}r_{jk}$ , where  $Q_{jk}$  represents the mass excess, or the amount of energy released when transforming a nucleus of type  $j$  into a nucleus of type  $k$ ).  $\varepsilon_v$  is the energy loss rate due to emission of neutrinos (typically taken from [121] or from [148], or from earlier work by the Japanese group). The mean molecular weight  $\mu$  is given by the following expression:

$$\mu = \frac{\rho}{m_{\text{amu}}} \sum_i [1 + v_e(i)] \frac{X_i}{A_i}, \quad (11)$$

where  $X_i$  indicates the chemical abundance by mass fraction of the  $i$ -th chemical element present in the stellar interior (whose atomic mass and number are  $A_i$  and  $Z_i$ , respectively), and  $v_e(i)$  is the number of free electrons contributed by one average particle

---

<sup>2</sup> The EOS by A. W. Irwin mentioned in [274] and currently in use by several different groups can be found in <http://sourceforge.net/projects/freeeos> and <ftp://astroftp.phys.uvic.ca/pub/irwin/eos/>.

of type  $i$ . Under suitable use of the Boltzmann and Saha equations (including, as may be indispensable in the stellar interior, the appropriate Coulomb corrections), one is able to compute  $v_e(i)$ , and hence  $\mu$ , at every point in the interior of a star, as needed for integration of the above system of equations. The importance of the Saha equation is that it allows one to compute the fractions of each element under different ionization stages as a function of the local temperature and density.

Time evolution in the abundance of element  $i$  is then given by the following equation:

$$\frac{\partial X_i}{\partial t} = \frac{m_i}{\rho} \left( \sum_j r_{ji} - \sum_k r_{ik} \right), \quad (12)$$

subject to the constraint  $\sum_i X_i = 1$ .

Note that it is common practice, in stellar interiors work, to characterize the chemical composition of a star using only three numbers, namely  $X$ ,  $Y$ ,  $Z$  – which represent the mass fraction of hydrogen, helium, and all elements heavier than helium (or “metals,” in astronomical jargon), respectively. In this case, the proportions of the different “metals” are usually taken to be the solar ones. In the case of the elements formed by successive captures of  $\alpha$  particles (helium nuclei), namely O, Ne, Mg, Si, S, Ca, and Ti, which for spheroids are found to present non-solar abundance ratios (e.g., [281, 286]), it has been shown that a simple rescaling of  $Z$  that takes into account the  $\alpha$ -element overabundance, according to  $Z = Z_0(0.638 f_\alpha + 0.362)$  – where  $Z_0$  is the solar-scaled metallicity,  $Z$  is the metallicity after account is taken of the  $\alpha$ -element overabundance, and  $f_\alpha$  is the  $\alpha$ -element overabundance factor – is sufficient for the computation of models that look morphologically very similar in the  $\log L - \log T_{\text{eff}}$  diagram (hereafter Hertzsprung-Russell diagram, or simply HRD), at least for metallicities  $Z \lesssim 3 \times 10^{-3}$  ([225, 274]; but see also §3.7 below for caveats regarding the extension of this result to the empirical color-magnitude diagram, hereafter CMD for short).

The preceding discussion shows how eqs. (6), (9), and (10) can be used to build a stellar structure model and evolve it in time. How do the other constitutive equations enter the picture? In order to answer this question, we must first take a look at how energy is transported in stellar interiors.

### 3.3. Energy Transport in the Stellar Interior

In stars, under normal circumstances, there is a steady flow of energy from the innermost regions, where thermonuclear reactions take place, to the outermost regions – and, eventually, from the latter to the interstellar space. Depending on the thermodynamical properties of the matter, such energy transport can occur in three different ways: by *radiative transfer*, which describes the transport of energy from hotter to cooler regions by photons as they interact with matter; by *convective motions*, which are macroscopic (usually turbulent) fluid motions which set in, under non-degenerate conditions, when radiative transport is incapable of taking care of the energy transport by itself; and by *conductive transfer*, which becomes very efficient under degenerate conditions but is usually quite negligible otherwise.

### 3.3.1. Radiative Transport

Under conditions of *radiative equilibrium*, when essentially all the energy is transported outwards by photons, it can be shown that the temperature gradient in eq. (5) takes the form

$$\nabla_{\text{rad}} = \frac{3}{16\pi acG} \frac{\overline{\kappa_R} LP}{mT^4}, \quad (13)$$

where  $a$  is the radiation constant,  $c$  is the speed of light in a vacuum, and  $\overline{\kappa_R}$  is the so-called *Rosseland mean opacity*. The latter is computed, on the basis of monochromatic opacities, from the following expression:

$$\frac{1}{\overline{\kappa_R}} = \frac{\int_0^\infty \frac{1}{\kappa_v} \frac{\partial B_v}{\partial T} dv}{\int_0^\infty \frac{\partial B_v}{\partial T} dv}. \quad (14)$$

Here  $v$  is the frequency, and  $B_v$  is the monochromatic Planck function. Tabulations of Rosseland mean opacities from the OPAL<sup>3</sup> (e.g., [147]) and OP<sup>4</sup> ([240, 8] and reference therein) groups are available in the literature and on the groups' respective web sites, and are almost exclusively employed in state-of-the-art stellar structure and evolution models, except for very low temperatures where molecular effects not treated in sufficient detail by OP and OPAL become important. In the latter case, of particular importance when dealing with stellar envelopes and atmospheres, the opacities by Alexander & Ferguson ([1]) are generally used. We will come back to the subject of radiative opacities momentarily.

Let us first take a look at the radiation transport equation at a given point in the stellar interior. Consider a point in the star at a distance  $r$  from the center. Then the amount of energy that flows through a cylinder of length  $d\ell$  inclined by an angle  $\theta$  with respect to the radial vector (Fig. 1) is given by the balance among four different terms: first, the radiation that enters the base of the cylinder, given by  $I(r, \theta)$ ; second, the radiation that is lost from the top of cylinder, given by  $I(r + dr, \theta + d\theta)$ ; third, the radiation gains due to emission inside the cylinder, given by  $dI = jd\ell = e\rho d\ell / (4\pi)$ , where  $j$  is the emission coefficient and  $e$  is the emissivity (assumed isotropic); fourth, the radiation losses due to absorption inside the cylinder, given by  $dI = -\alpha I(r, \theta) d\ell = -\kappa \rho I(r, \theta) d\ell$ , where  $\alpha$  is the absorption coefficient and  $\kappa$  is the opacity. From this, it follows that the *energy* that is lost per unit time from inside the cylinder due to absorption is  $-\kappa \rho d\ell I d\Omega dS$  (where  $S$  is the area of the base, and  $\Omega$  the associated solid angle), whereas the amount of energy gained per unit time due to the emissivity is  $e\rho d\ell dS d\Omega / (4\pi)$ . Naturally, the difference between these two terms must equal  $[I(r + dr, \theta + d\theta) - I(r, \theta)] d\Omega dS$ . Therefore, one has:

---

<sup>3</sup> OPAL: <http://www-phys.llnl.gov/Research/OPAL/opal.html>

<sup>4</sup> OP: <http://vizier.u-strasbg.fr/OP.html>

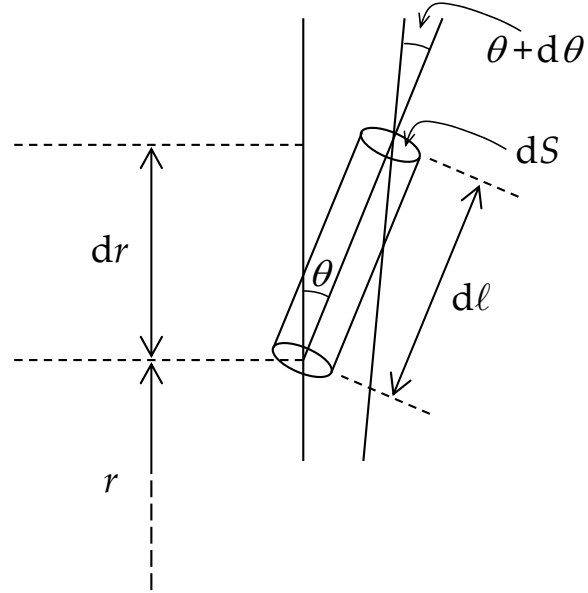


**FIGURE 1.** Basic geometric quantities used in the definition of the radiative temperature gradient. Adapted from [234], which in turn is based on the discussion in §73 in [96].

$$I(r + dr, \theta + d\theta) - I(r, \theta) = \frac{e\rho d\ell}{4\pi} - I(r, \theta) \kappa \rho d\ell, \quad (15)$$

which can also be written as

$$\frac{\partial I}{\partial r} dr + \frac{\partial I}{\partial \theta} d\theta = \frac{e\rho d\ell}{4\pi} - I \kappa \rho d\ell. \quad (16)$$

We must get rid of either  $\ell$  or  $r$  in order to put this equation into a useful form – and, of course, we choose to keep the latter. Noting the geometrical relations (see Fig. 1)

$$dr = d\ell \cos \theta \quad \text{and} \quad -d\theta = \frac{d\ell \sin \theta}{r}, \quad (17)$$

one easily arrives at the following differential equation:

$$\frac{\partial I}{\partial r} \cos \theta - \frac{\partial I}{\partial \theta} \frac{\sin \theta}{r} + I \kappa \rho - \frac{e\rho}{4\pi} = 0. \quad (18)$$

Since the only radiation field-related quantity that enters the set of eqs. (1)-(4) is the luminosity, which in turn is related to the radiation flux by the geometric relation  $F = L/(4\pi r^2)$ , we can transform the above equation into a more useful form that uses directly the flux. We achieve this goal by recalling the definition of flux, namely,

$$F(r) \equiv \int_{\Omega} I(r, \theta) \cos \theta d\Omega. \quad (19)$$

We must accordingly replace the intensity with the flux in eq. (18), which we achieve by multiplying the latter by  $d\Omega$  and integrating over all solid angles. We get:

$$\frac{\partial}{\partial r} \int_{\Omega} I \cos \theta d\Omega - \frac{1}{r} \int_{\Omega} \frac{\partial I}{\partial \theta} \sin \theta d\Omega + \kappa \rho \int_{\Omega} I d\Omega - \frac{e\rho}{4\pi} \int_{\Omega} d\Omega = 0. \quad (20)$$

It is easy to show that, in fact,

$$\int_{\Omega} \frac{\partial I}{\partial \theta} \sin \theta d\Omega = -2F; \quad (21)$$

recalling the definition of energy density  $u(r)$  as the zero-th order moment of the radiation field over the speed of light  $c$ , we then have:

$$\frac{\partial F}{\partial r} + \frac{2F}{r} + \kappa \rho c u - e\rho = 0. \quad (22)$$

While we have succeeded in getting rid of the intensity and bringing the flux into our formalism, we have unfortunately introduced another quantity which we (still) do not know how to compute from the thermodynamic properties of the medium, namely, the energy density  $u$ . We thus need at least one additional relationship involving the energy density in order to be able to solve eq. (22). We can obtain one such relation by multiplying eq. (18) by  $\cos \theta d\Omega$  and again integrating over all solid angles. In this way, and recalling that the radiation pressure  $P_R$  is the second moment of the radiation field (over  $c$ ), we get:

$$\frac{\partial P_R}{\partial r} + \frac{3P_R - u}{r} + \frac{\kappa \rho F}{c} = 0. \quad (23)$$

Again, we have achieved our goal of eliminating  $u$  from the differential equation – but only at the expense of adding in yet another unknown quantity, namely the radiation pressure. We could multiply yet again eq. (18) by  $\cos^2 \theta d\Omega$  and integrate over all solid angles, but this will again add in a higher-order moment of the radiation field – and so on and so forth.

A particularly elegant way out of this conundrum is to analyze the convergence of a cosine series expansion of the radiation field at a given point in the stellar interior:

$$I(r, \theta) = I_0(r) + \sum_{n=1}^{\infty} I_n(r) \cos^n \theta. \quad (24)$$

In a typical stellar interior, this series converges extremely rapidly (see §75 in [96], or §II.6 in [234]), with a typical convergence rate given by

$$\left| \frac{I_{n+1}}{I_n} \right| \sim 10^{-10}, \quad (25)$$

which allows us to ignore the higher-order terms in this expansion with very high accuracy. Therefore, we take, with sufficient accuracy,

$$I(r, \theta) \simeq I_0(r) + I_1(r) \cos \theta. \quad (26)$$

In this case, the energy density, the flux, and the radiation pressure assume the following values:

$$u(r) = \frac{4\pi}{c} I_0(r), \quad (27)$$

$$F(r) = \frac{4\pi}{3} I_1(r), \quad (28)$$

$$P_R(r) = \frac{4\pi}{3c} I_0(r). \quad (29)$$

From this, it is immediately clear that  $P_R = u/3$ . It is also apparent that the energy density depends only on the isotropic component of the radiation field (higher-order contributions to eq. [27] typically being many orders of magnitude smaller than the zero-order term, and hence totally negligible). Conversely, the radiation flux depends only on the degree of anisotropy of the radiation field. Small as the latter may be in stellar interiors, it is absolutely crucial in terms of the structure of the star and its very existence as a visible object!

What are the values of  $I_0$  and  $I_1$ ? Since  $u$  is the energy density of the radiation field, and since conditions of thermal equilibrium hold to excellent approximation in stellar interiors, it is natural to identify  $I_0$  with the thermal (Planck) contribution, which is given by

$$I_0 = \int_0^\infty B_\nu(T) d\nu = \frac{ac}{4\pi} T^4. \quad (30)$$

Therefore,

$$u = aT^4, \quad (31)$$

$$P_R = \frac{aT^4}{3}, \quad (32)$$

which implies, according to eq. (23),

$$\frac{\partial P_R}{\partial r} + \frac{\kappa \rho F}{c} = 0. \quad (33)$$

According to eq. (32), then,

$$F = -\frac{4ac}{3\kappa\rho} T^3 \frac{\partial T}{\partial r}, \quad (34)$$

or, in terms of the luminosity,

$$L = -\frac{16\pi acr^2}{3\kappa\rho} T^3 \frac{\partial T}{\partial r}. \quad (35)$$

Recalling the definition of logarithmic temperature gradient (eq. 5), and bearing in mind the chain rule of calculus, one has

$$\frac{\partial T}{\partial r} = \frac{\partial T}{\partial P} \frac{\partial P}{\partial r} = \frac{T}{P} \frac{\partial \ln T}{\partial \ln P} \frac{\partial P}{\partial r} = \frac{T}{P} \frac{\partial P}{\partial r} \nabla_{\text{rad}}. \quad (36)$$

But we actually know the value of the pressure gradient from our hypothesis of hydrostatic equilibrium (eq. 2), which in the Eulerian form reads  $\partial P/\partial r = -Gm\rho/r^2$ ; therefore,

$$\frac{\partial T}{\partial r} = -\frac{Gm\rho T}{r^2 P} \nabla_{\text{rad}}, \quad (37)$$

which, together with eq. (35), gives

$$\nabla_{\text{rad}} = \frac{3\kappa PL}{16\pi acGmT^4}, \quad (38)$$

which is the desired expression for the temperature gradient in the stellar interior when the energy is transported outwards by radiation. This, of course, is the same as eq. (13), showing also that the opacity that appears in eq. (38) is in fact the Rosseland mean (eq. 14).

### 3.3.2. Convective Transport

When the temperature gradient indicated by eq. (13) or (38) is too steep, radiation may be unable to carry away all of the energy outwards by itself. When this happens, convective instabilities set in, and the hypothesis of radiative equilibrium breaks down.<sup>5</sup> In what follows, we shall describe the basic theory of convective transport in stellar interiors, first establishing the commonly adopted criteria for the onset of the instability, and then describing how to compute the value of  $\nabla$  in eq. (5) using the mixing-length theory of convection.

#### Criteria for the Onset of Convective Instabilities

Let us analyze the conditions under which convective instabilities may set in in the stellar interior. With this purpose in mind, we consider the displacement of a random fluctuation or “bubble” that forms inside the star, and consider whether the bubble, after a small displacement, tends to move back to its original position (in which case the instability cannot set in) or instead tends to keep on moving farther away from its initial position (in which case convective instability ensues).

The situation is shown schematically in Fig. 2. The bubble is originally indistinguishable from its surroundings, so that its initial thermodynamic properties and those of the surrounding medium are the same, and can be characterized by the pressure  $P_0$ , density  $\rho_0$ , and mean molecular weight  $\mu_0$ . After a small displacement upwards by a distance  $\Delta r$ , the bubble’s thermodynamic state is described by the quantities  $P_{\text{bub}}$ ,  $\rho_{\text{bub}}$ , and  $\mu_{\text{bub}}$ , whereas the state of the surroundings is described instead by  $P_{\text{sur}}$ ,  $\rho_{\text{sur}}$ ,  $\mu_{\text{sur}}$ . Clearly, by

---

<sup>5</sup> Very interesting discussions of the physical conditions under which this occurs have been presented in [146, 93], where it is argued, on the basis of the so-called *Naur-Osterbrock criterion* ([266, 179]), that it is the derivatives of the energy generation rates and radiative opacities with  $T$  and  $\rho$  that define whether a convective core will indeed exist or not.

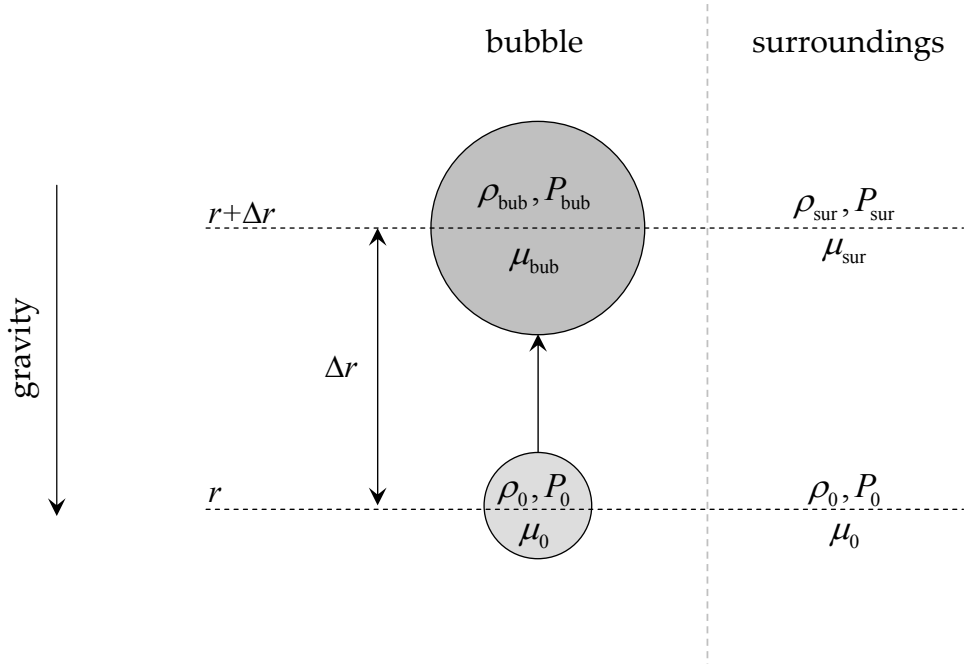


**FIGURE 2.** Schematic description of quantities related to the treatment of convective instabilities in the stellar interior. In gray is shown a convective bubble element, which is initially in equilibrium with its surroundings (initial conditions are denoted with a subscript “0”). After a displacement by a distance  $\Delta r$ , the bubble’s thermodynamic state will be described by the variables  $\rho_{\text{bub}}$ ,  $P_{\text{bub}}$ ,  $\mu_{\text{bub}}$ , whereas its surroundings are described instead by  $\rho_{\text{sur}}$ ,  $P_{\text{sur}}$ ,  $\mu_{\text{sur}}$ .

the Archimedes Principle, the bubble will continue moving upwards, and hence convective instability set in, if

$$\rho_{\text{bub}} < \rho_{\text{sur}}, \quad (39)$$

or, equivalently,

$$\frac{d\rho_{\text{bub}}}{dr} - \frac{d\rho_{\text{sur}}}{dr} < 0. \quad (40)$$

It is easy to see that, as a consequence of the EOS (eq. 6), this sets a limit on the rate of variation of the temperature gradient inside the star (the pressure gradient is already specified by the hydrostatic equilibrium condition, eq. 2). We can make further progress by noting that, provided the speed of sound is sufficiently high compared with the displacement velocity of the bubble, the latter is always capable of keeping pressure equilibrium with its surroundings. [Indeed, according to the recent calculations by [32], supersonic convection does not occur in the case of low-mass stars, except perhaps at its high-mass end (§1); see his Fig. 1.] Based on this assumption, let us compute the requirement on the temperature gradient explicitly (similar discussions can be found in [153, 223]).

First, note that the net acceleration of the bubble can be computed, if viscous drag forces can be ignored, from the following expression:

$$\frac{d^2\Delta R}{dt^2} = -g - \frac{1}{\rho} \frac{dP}{dr}; \quad (41)$$

now taking into account the fact that  $\Delta r$  is a small displacement, one may write  $\rho = \rho_0(1 + \Delta\rho/\rho_0)$  (where  $\Delta\rho \equiv \rho_{\text{bub}} - \rho_{\text{sur}}$ ). Therefore, to first order, one has

$$\frac{d^2\Delta R}{dr^2} = -g - \frac{1}{\rho_0 \left(1 + \frac{\Delta\rho}{\rho_0}\right)} \frac{dP}{dr} \quad (42)$$

$$\simeq -g_0 - \frac{1}{\rho_0} \left( \frac{dP}{dr} \right)_0 \left( 1 - \frac{\Delta\rho}{\rho_0} \right) \quad (43)$$

$$= -g_0 - \frac{1}{\rho_0} \left( \frac{dP}{dr} \right)_0 + \frac{1}{\rho_0} \left( \frac{dP}{dr} \right)_0 \frac{\Delta\rho}{\rho_0} \quad (44)$$

$$= -g_0 \frac{\Delta\rho}{\rho_0}, \quad (45)$$

where we have used the fact that the bubble is initially in equilibrium, i.e.,

$$\left( \frac{d^2\Delta R}{dr^2} \right)_0 = -g_0 - \frac{1}{\rho_0} \left( \frac{dP}{dr} \right)_0 = 0. \quad (46)$$

Therefore, dropping subscripts, one may write, to first order,

$$\frac{d^2\Delta R}{dr^2} = -g \frac{\Delta\rho}{\rho}. \quad (47)$$

We can obtain additional differential equations describing the time behavior of the thermodynamic properties of our bubble as follows. For the mean molecular weight, one has

$$\Delta\mu \equiv \mu_{\text{bub}} - \mu_{\text{sur}} = \mu_0 - \left( \mu_0 + \frac{d\mu}{dr} \Delta r \right) = -\frac{d\mu}{dr} \Delta r, \quad (48)$$

which, using the chain rule and also considering that the evolutionary timescales are always much longer than the convective instability timescales, can also be written as

$$\frac{d\Delta\mu}{dt} = -\frac{d}{dt} \left( \frac{d\mu}{dr} \Delta r \right) = -\mu \frac{d \ln \mu}{d \ln P} \frac{d \ln P}{dr} \frac{d \Delta r}{dt} = \mu \nabla_\mu \lambda_p^{-1} \frac{d \Delta r}{dt}, \quad (49)$$

which is the desired equation for the perturbation in  $\mu$ , and where we have defined  $\nabla_\mu \equiv d \ln \mu / d \ln P$  and the *pressure scale height*  $\lambda_p^{-1} \equiv -P^{-1} dP/dr$ . Likewise, for  $T$ , we define

$$\Delta T \equiv T_{\text{bub}} - T_{\text{sur}} = \left[ \left( \frac{dT}{dr} \right)_{\text{ad}} - \left( \frac{dT}{dr} \right)_{\text{rad}} \right] \Delta r - \beta \Delta T dt. \quad (50)$$

In this equation, the temperature gradient that would be present if the displacement of the bubble were precisely adiabatic (i.e., if the bubble did not exchange any heat with its surroundings) is denoted by  $(dT/dr)_{\text{ad}}$ ; since Nature is never precisely adiabatic, we have also taken into account non-adiabatic effects by adding in the second term on the right, where one can see that  $\beta\Delta T$  is the rate of temperature change due to the bubble's energy losses. Obviously, the adiabatic case corresponds to  $\beta = 0$ .

Taking the time derivative of eq. (50), and again applying the chain rule, one gets

$$\frac{d\Delta T}{dt} = -T\lambda_P^{-1} \left[ \left( \frac{d \ln T}{d \ln P} \right)_{\text{ad}} - \left( \frac{d \ln T}{d \ln P} \right)_{\text{rad}} \right] \frac{d\Delta r}{dt} - \beta\Delta T; \quad (51)$$

recalling the definition of  $\nabla$  (eq. 5), one then finds

$$\frac{d\Delta T}{dt} = -T\lambda_P^{-1} (\nabla_{\text{ad}} - \nabla_{\text{rad}}) \frac{d\Delta r}{dt} - \beta\Delta T. \quad (52)$$

We now have a system of three differential equations describing the time evolution of the four unknowns  $\Delta r, \Delta\rho, \Delta\mu, \Delta T$ . A fourth relation is provided by the EOS, which dictates that the changes in the thermodynamical properties of a system must be related as

$$-\frac{\Delta P}{P} + \chi_\rho \frac{\Delta\rho}{\rho} + \chi_T \frac{\Delta T}{T} + \chi_\mu \frac{\Delta\mu}{\mu} = 0, \quad (53)$$

where

$$\chi_\rho \equiv \left( \frac{d \ln P}{d \ln \rho} \right)_{T,\mu}, \quad \chi_T \equiv \left( \frac{d \ln P}{d \ln T} \right)_{\rho,\mu}, \quad \chi_\mu \equiv \left( \frac{d \ln P}{d \ln \mu} \right)_{\rho,T}. \quad (54)$$

For instance, for an ideal gas EOS, one can easily see that  $\chi_\rho = \chi_T = -\chi_\mu = 1$ . Since the bubble always keeps pressure equilibrium with its surroundings, eq. (53) simplifies to

$$\chi_\rho \frac{\Delta\rho}{\rho} + \chi_T \frac{\Delta T}{T} + \chi_\mu \frac{\Delta\mu}{\mu} = 0, \quad (55)$$

which is the fourth equation that we were seeking.

Our system of four equations given by eqs. (47), (49), (52), and (55) is in fact quite complex, so instead of studying the full motion of the convective bubble we simply check whether solutions of the form

$$\Delta y = A_y e^{vt}, \quad (56)$$

where  $A_y$  is a constant and  $v$  is a frequency, are possible. Inserting this proposed solution into the aforementioned equations, we get:

$$gA_\rho e^{vt} + \rho v^2 A_r e^{vt} = 0, \quad (57)$$

$$vA_\mu e^{vt} - \mu \nabla_\mu \lambda_P^{-1} v A_r e^{vt} = 0, \quad (58)$$

$$vA_T e^{vt} - T \lambda_P^{-1} (\nabla_{\text{rad}} - \nabla_{\text{ad}}) v A_r e^{vt} + \beta A_T e^{vt} = 0, \quad (59)$$

$$\chi_\rho \frac{A_\rho}{\rho} + \chi_T \frac{A_T}{T} + \chi_\mu \frac{A_\mu}{\mu} = 0. \quad (60)$$

Now, in order to ensure that a non-trivial solution exists, the determinant formed by the  $A_x$  coefficients must be zero; thus:

$$\begin{vmatrix} 0 & g & 0 & \rho v^2 \\ 0 & 0 & v & -v\mu\lambda_P^{-1}\nabla_\mu \\ v + \beta & 0 & 0 & -vT\lambda_P^{-1}(\nabla_{\text{rad}} - \nabla_{\text{ad}}) \\ \frac{\chi_T}{T} & \frac{\chi_\rho}{\rho} & \frac{\chi_\mu}{\mu} & 0 \end{vmatrix} = 0. \quad (61)$$

This leads to the following dispersion relation:

$$v^3 + v^2\beta - v \left[ g\lambda_P^{-1} \frac{\chi_T}{\chi_\rho} \left( \nabla_{\text{rad}} - \nabla_{\text{ad}} + \frac{\chi_\mu}{\chi_T} \nabla_\mu \right) \right] - g\lambda_P^{-1} \beta \frac{\chi_\mu}{\chi_\rho} \nabla_\mu = 0. \quad (62)$$

In particular, in the adiabatic case ( $\beta = 0$ ), this reduces to

$$v^2 = g\lambda_P^{-1} \frac{\chi_T}{\chi_\rho} \left( \nabla_{\text{rad}} - \nabla_{\text{ad}} + \frac{\chi_\mu}{\chi_T} \nabla_\mu \right), \quad (63)$$

which corresponds to the so-called *Brunt-Väisälä* (or buoyancy) frequency, first derived in the context of oscillations of planetary atmospheres by [270] and, independently, by [28]. In this sense, this quantity plays a particularly important role in the theory of non-radial oscillations of stars: note that, for  $v^2 < 0$ , the Brunt-Väisälä frequency is purely imaginary, and eq. (56) indicates a purely oscillatory motion – which is related to the  $g$ -modes of non-radial pulsations (see, e.g., [106] and references therein). We are not chiefly preoccupied with oscillations of stars though; our interest is focused instead on the possibility of real and *positive* values of  $v$ , since eq. (56) indicates to us that, in this case, our initially very small perturbations will actually grow exponentially over time, thus giving rise to convective instability. Therefore, in order for convective motions to set in in the adiabatic case, one needs

$$\nabla_{\text{rad}} > \nabla_{\text{ad}} - \frac{\chi_\mu}{\chi_T} \nabla_\mu. \quad (64)$$

This is the so-called *Ledoux criterion*, first derived by Ledoux in 1947 ([167]). Note that the mean molecular weight gradient that appears in this equation must be treated with care; according to [76], in particular, molecular weight gradients that are solely due

to ionization effects should not be taken into account when using this equation, since ionization effects are already implicitly taken into account in the EOS.

In the special case where there is no chemical composition gradient,  $d \ln \mu / d \ln P = 0$ , and the Ledoux criterion reduces to

$$\nabla_{\text{rad}} > \nabla_{\text{ad}}, \quad (65)$$

which is the well-known *Schwarzschild criterion* ([233]) for the onset of convective instability. This is – by far – the most applied convective instability criterion in actual stellar structure calculations. The way it is usually employed is as follows: first, one integrates the set of equations (1)-(4), assuming radiative equilibrium; this gives us  $\nabla_{\text{rad}}$  at each point in the star. In parallel, one also computes the adiabatic gradient  $\nabla_{\text{ad}}$  at each point, and then compares the two. If the inequality (65) is satisfied, then the radiative temperature gradient is incorrect, and a different recipe must be used, taking into account convective energy transport, to define the new temperature gradient. Note that  $\nabla_{\text{ad}}$  can be computed from the properties of adiabatic transformations; in other words,

$$\nabla_{\text{ad}} = \left( \frac{d \ln T}{d \ln P} \right)_{\text{ad}} = 1 - \frac{1}{\Gamma_2}, \quad (66)$$

where  $\Gamma_2$  is the *second adiabatic exponent*, which can be computed on the basis of the thermodynamic properties of the matter [e.g., eqs. (6) and (7)]. For instance, in the special case of an ideal gas, one has  $\Gamma_2 = c_P/c_V$ , where  $c_V$  is the specific heat at constant volume (see §9.14 in [76] for further details).

It should be noted that, although we derived eqs. (64) and (65) taking  $\beta = 0$  (i.e., in the adiabatic case), it is also possible to arrive at these results on the basis of the dispersion relation eq. (62): as shown in [223], solutions of this equation containing a positive real part (i.e., indicating a growing perturbation and hence the onset of instability) are obtained if either eq. (64) or eq. (65) are satisfied, and also if

$$\frac{d \ln \mu}{d r} > 0. \quad (67)$$

This is the well-known *Rayleigh-Taylor instability*, which basically states that layers of matter with a higher molecular weight cannot exist in equilibrium on top of layers with lower molecular weight. In the case of low-mass stars, it has recently been suggested ([97]), on the basis of 3D models, that this instability may be important for reliable predictions of the stellar nucleosynthesis and Galactic evolution of  $^3\text{He}$ , which plays a key role in the context of empirical tests of Big Bang nucleosynthesis (e.g., [125], [182]). On the other hand, it should be noted that [97] did not actually follow the mixing through the radiative zone above the hydrogen shell, but only speculated that such mixing should reach the convective envelope on a short timescale. Moreover, they started their calculations with a model already well up the RGB in which previous mixing was not considered (because these models were carried out in 1D). Clearly, additional work will be required before putting their results on a firmer footing.

### The Temperature Gradient under Convective Stability

The Schwarzschild and Ledoux criteria tell us, for each point in the star, whether it is in radiative equilibrium or not. If it is, the temperature gradient is immediately given by eq. (13). What is the temperature gradient when radiative equilibrium does *not* hold – i.e., when convection also becomes an efficient mechanism of energy transport?

In order to answer this question, we must study in more detail the properties of the convective bubbles shown in Fig. 2. More specifically, we must know the excess heat contained in the bubble, as well as its displacement speed and, of course, the distance traversed before it imparts its excess heat to its surroundings. The way this is usually accomplished, in stellar interiors work, is using the so-called *mixing length theory* of convection, as originally formulated by [278, 22] (for alternative formulations of this theory, see also, e.g., [128, 185]).

Turbulent convection is one of the most complicated problems in physics. However, within the scope of the mixing length theory, a number of approximations are made which make the problem more tractable. In particular, one first assumes that the full spectrum of eddies that normally characterizes a turbulent flow can be described in terms of a single, “representative” bubble. Second, one assumes that this bubble will traverse a distance  $\ell$  – the mixing length – before finally dissolving and giving out its excess heat to the surroundings. Third, it is assumed that the bubble preserves its physical identity throughout its displacement by the distance  $\ell$ . Fourth, the bubble is also assumed to keep pressure equilibrium with its surroundings during the whole process. Fifth, viscous forces are assumed to be negligible. These and other approximations are discussed, for instance, in [168, 76, 250, 75, 37, 123].

Let us first compute the excess heat  $\Delta Q$  contained, per unit volume, within this convective element or “bubble” (Fig. 2). Since the bubble keeps pressure equilibrium with its surroundings until the moment when it gives out its excess heat, we have

$$\Delta Q = \rho c_P \Delta T, \quad (68)$$

where  $\Delta T$  is  $T_{\text{bub}} - T_{\text{sur}}$ . Note that  $\Delta T$  can also be written as

$$\Delta T = \left[ \left( \frac{dT}{dr} \right)_{\text{bub}} - \left( \frac{dT}{dr} \right)_{\text{sur}} \right] \Delta r; \quad (69)$$

therefore, defining

$$\Delta \nabla T \equiv \left( \frac{dT}{dr} \right)_{\text{bub}} - \left( \frac{dT}{dr} \right)_{\text{sur}}, \quad (70)$$

one finds

$$\Delta T = \Delta \nabla T \Delta r, \quad (71)$$

and therefore

$$\Delta Q = \rho c_P \Delta \nabla T \Delta r. \quad (72)$$

We note, in passing, that  $\Delta \nabla T$  can also be written as

$$\Delta\nabla T = \left[ \left( \frac{dT}{dP} \right)_{\text{bub}} - \left( \frac{dT}{dP} \right)_{\text{sur}} \right] \frac{dP}{dr} \quad (73)$$

$$= \left[ \left( \frac{d \ln T}{d \ln P} \right)_{\text{bub}} - \left( \frac{d \ln T}{d \ln P} \right)_{\text{sur}} \right] \frac{T}{P} \frac{dP}{dr} \quad (74)$$

$$= (\nabla_{\text{bub}} - \nabla_{\text{sur}}) \frac{T}{P} \frac{dP}{dr} \quad (75)$$

$$= (\nabla_{\text{sur}} - \nabla_{\text{bub}}) T \frac{\Delta r}{\lambda_P}. \quad (76)$$

Before proceeding, we must emphasize that the temperature gradients that appear in these equations are (in general) *not* the same as those appearing in eq. (50). The four gradients should be interpreted as follows:  $\nabla_{\text{rad}}$  is the gradient that would be present under radiative equilibrium.  $\nabla_{\text{ad}}$  is the temperature gradient in the bubble if its displacement were adiabatic, i.e., if it did not exchange any heat with its surroundings during its ascent.  $\nabla_{\text{bub}}$  is the actual temperature gradient in the bubble, which will be equal to  $\nabla_{\text{ad}}$  only if the bubble's displacement is adiabatic. Finally,  $\nabla_{\text{sur}}$  is the temperature gradient in the surroundings of the bubble – in the preceding equilibrium discussion, this meant the radiative gradient, since we were discussing under which conditions the bubble's initial (small) motion would *lead* to a convective instability; in the present discussion, on the other hand, this stands for the *actual* temperature gradient that is present in the surroundings of the convective element, when the convective instability is *already* fully developed.

Now the actual heat *flux* depends on the velocity of the bubble, which can in principle be computed by integrating the equation of motion [i.e., eq. (41) or (47)]. Instead of doing this, we note that the average force acting on the bubble (per unit volume), while it traverses the distance  $\Delta r$ , is given by

$$\langle \mathcal{F} \rangle \simeq \frac{1}{2} g \Delta \rho, \quad (77)$$

where the factor 1/2 is due to the fact that  $\Delta \rho/2$  is the average density difference between the bubble and the surroundings, since we assume that, initially, the bubble and the surroundings are basically indistinguishable (see Fig. 2) and, moreover, eq. (47) implies that  $\Delta \rho$ , to first order, increases linearly with  $\Delta r$ . Now, in analogy with eq. (74),  $\Delta \rho$  can be computed from

$$\Delta \rho = \left[ \left( \frac{d \ln \rho}{d \ln P} \right)_{\text{bub}} - \left( \frac{d \ln \rho}{d \ln P} \right)_{\text{sur}} \right] \frac{\rho}{P} \frac{dP}{dr} \Delta r. \quad (78)$$

The convective energy flux can be computed from the foregoing equations more generally, but it is instructive to see what happens when we assume that the motion of the bubble *is* adiabatic, and ignoring molecular weight gradients (which, in any case, convection quickly tends to smooth out). In this case, keeping in mind eq. (66) and recalling that  $P \propto \rho^{\Gamma_2}$  for an adiabatic transformation, one finds

$$\left(\frac{d \ln \rho}{d \ln P}\right)_{\text{bub}} = \left(\frac{d \ln \rho}{d \ln P}\right)_{\text{ad}} = \frac{1}{\Gamma_2} = 1 - \nabla_{\text{ad}}. \quad (79)$$

Evaluating this derivative for the surroundings is more complicated, since here we have to resort to the more general relation eq. (53). In this case, one finds

$$\left(\frac{d \ln \rho}{d \ln P}\right)_{\text{sur}} = \frac{1}{\chi_{\rho}} - \frac{\chi_T}{\chi_{\rho}} \left(\frac{d \ln T}{d \ln P}\right)_{\text{sur}} - \frac{\chi_{\mu}}{\chi_{\rho}} \left(\frac{d \ln \mu}{d \ln P}\right)_{\text{sur}}. \quad (80)$$

Therefore, in this case, ignoring molecular weight gradients, and recalling the definition eq. (5), one finds

$$\left(\frac{d \ln \rho}{d \ln P}\right)_{\text{sur}} = \frac{1}{\chi_{\rho}} - \frac{\chi_T}{\chi_{\rho}} \nabla_{\text{sur}}. \quad (81)$$

Dropping subscripts for the surrounding quantities, one then has

$$\Delta \rho = \left[ (1 - \nabla_{\text{ad}}) - \left( \chi_{\rho}^{-1} - \frac{\chi_T}{\chi_{\rho}} \nabla \right) \right] \frac{\rho}{P} \frac{dP}{dr} \Delta r \quad (82)$$

$$= \left[ \left( 1 - \chi_{\rho}^{-1} \right) + \left( \frac{\chi_T}{\chi_{\rho}} \nabla - \nabla_{\text{ad}} \right) \right] \frac{\rho}{P} \frac{dP}{dr} \Delta r \quad (83)$$

$$= - \left[ \left( 1 - \chi_{\rho}^{-1} \right) + \left( \frac{\chi_T}{\chi_{\rho}} \nabla - \nabla_{\text{ad}} \right) \right] \rho \frac{\Delta r}{\lambda_P}. \quad (84)$$

This takes on a particularly simple form in the case of an ideal gas, when  $\chi_T = \chi_{\rho} = 1$ . In this case, eq. (84) reduces to (see eq. 76, and recall that we are assuming that the bubble's displacement is adiabatic)

$$\Delta \rho = - (\nabla - \nabla_{\text{ad}}) \rho \frac{\Delta r}{\lambda_P} = - \frac{\rho}{P} \Delta \nabla T \Delta r, \quad (85)$$

so that the average force (eq. 77) becomes

$$\langle \mathcal{F} \rangle \simeq \frac{g \rho}{2T} \Delta \nabla T \Delta r. \quad (86)$$

At a given instant of time, a typical bubble will have traversed a distance given by  $\Delta r \approx \ell/2$ , so that the average velocity can be computed from

$$\langle \mathcal{F} \rangle \Delta r = \frac{1}{2} \rho \langle v^2 \rangle \Rightarrow \langle v^2 \rangle \simeq \frac{g}{T} \Delta \nabla T \frac{\ell^2}{4}. \quad (87)$$

Therefore, from eqs. (72) and (87), and recognizing that there are about as many “hot” bubbles moving upwards as there are “cold” bubbles moving downwards, the convective energy flux is given by

$$F_{\text{conv}} = 2v \Delta Q \simeq \rho c_P \frac{\ell^2}{4} \left( \frac{g}{T} \right)^{\frac{1}{2}} (\Delta \nabla T)^{\frac{3}{2}}. \quad (88)$$

Except for a numerical factor of order unity – which is not of primary relevance in the context of the mixing length theory, since the value of  $\ell$  is still unspecified and must actually be calibrated by comparing the stellar model results (i.e., the predicted radii and effective temperatures) with the observations (i.e., the measured values for the Sun at its present age) – this expression is essentially identical to eq. (21.14) in [265], or to eq. (7.7) in [234], or also to eq. (14.31a) in [76].

In the convective cores of intermediate- and high-mass stars, where energy generation proceeds through the CNO cycle, the triple- $\alpha$  process, or even more advanced energy generation cycles (e.g., [71, 214]), one finds that the value of  $\Delta\nabla T$  appearing in this equation is very small. This means that convection is very efficient in these cases, but a minor superadiabaticity (i.e., deviation from the adiabatic regime) being needed in order to transport the excess heat from the energy-generating regions of the stars. Under such circumstances, since the two gradients are so similar, it is sufficient to take the adiabatic value for the actual temperature gradient in eq. 4. In the case of low-mass stars, this actually happens during the HB phase: for instance, adopting typical values for the core of an HB star from Fig. 11 in [140], one finds values of  $\Delta\nabla T \approx 2 \times 10^{-10} \text{ K cm}^{-1}$ , compared with an actual temperature gradient some six orders of magnitude higher, namely,  $dT/dr \approx 6 \times 10^{-4} \text{ K cm}^{-1}$ .

However, in order to properly describe the temperature profiles of the convective *envelopes* of low-mass stars, eq. (88) must be solved, together with the radiative transfer equation, for the *actual* temperature gradient. In this case, the total flux is given by the combination of radiative and convective fluxes, thus:

$$F = F_{\text{rad}} + F_{\text{conv}} = \frac{L}{4\pi r^2} = -\frac{4ac}{3\bar{\kappa}_R \rho T^3} \frac{dT}{dr} + \rho c_P \frac{\ell^2}{4} \left( \frac{g}{T} \right)^{\frac{1}{2}} \left[ \left( \frac{dT}{dr} \right)_{\text{ad}} - \left( \frac{dT}{dr} \right) \right]^{\frac{3}{2}}, \quad (89)$$

where we have used the definition of  $\Delta\nabla T$  as given in eq. (70), dropping the subscript “sur” for the actual temperature gradient, and assuming that the bubble does move along an adiabat in parameter space.

In order to solve this equation for the temperature gradient, one must know the mixing length  $\ell$ . What value does  $\ell$  take on? In the mixing length theory, this is usually taken as proportional to the pressure scale height  $\lambda_P$ , so that

$$\ell \equiv \alpha_\ell \lambda_P, \quad (90)$$

which corresponds to the definition of the *mixing length parameter*  $\alpha_\ell$ . The latter’s value will depend on one’s exact implementation of the mixing length theory, and even on the detailed opacity tables used [e.g., [65]; see the dependence on  $\bar{\kappa}_R$  in eq. (89)], so that it may be quite risky to compare values obtained by different authors without first making sure, among other things, that the numerical factor appearing in eq. (88) is the same for all, and that similar opacity tables have been used. In any case, typical values fall in the range  $1.5 \lesssim \alpha_\ell \lesssim 2.5$ , and are obtained by following the evolution of a one-solar-mass star with the same chemical composition as the Sun until the present (i.e., for  $4.57 \pm 0.05$  Gyr; see [9, 251]), and checking which value of  $\alpha_\ell$  better matches the observed properties of the Sun – especially its radius and temperature, which depend

crucially on the temperature profile of its outer envelope. One then *assumes* that the mixing length parameter is the same for every star, irrespective of its mass, chemical composition, or evolutionary phase. One may suspect that this may be too crude an approach for state-of-the-art, quantitative stellar evolutionary modelling – but in fact, this is still the procedure that is followed by the vast majority of workers in the field, and it does give, with virtually no additional assumptions, a surprisingly good description of the observations for stars in globular clusters (e.g., [101, 187, 99]).

### Overshooting, Semiconvection, and “Breathing Pulses”

The criteria we have derived above for the placement of the boundaries of a convection zone (eqs. 64 and 65) are strictly *local*, in the sense that they depend exclusively on the physical properties at the place we are studying. Nature, however, is more complicated than that; in particular, convective bubbles that are approaching the convective boundary set by either the Ledoux or the Schwarzschild criteria may retain sufficient momentum that they may be able to “overshoot” into the region that, according to those criteria, should be in radiative equilibrium. Since the bubble’s velocity at the formal convective border, and hence its ultimate fate, clearly depends on what happened to it *before* it reached this point, a description of overshooting must involve *non-local* phenomena. In this sense, convective overshooting is most frequently treated using the formalism developed by Roxburgh ([219, 220, 221]). In its simplest form ([220]), the actual extent of a convective region is determined by the values of  $r_{\text{inn}}$  and  $r_{\text{out}}$  (inner and outer radii of the convective region, respectively) which satisfy the following equation (the so-called “Roxburgh criterion”):

$$\int_{r_{\text{inn}}}^{r_{\text{out}}} (L_{\text{rad}} - L) \frac{1}{T^2} \frac{dT}{dr} dr = 0, \quad (91)$$

where  $L_{\text{rad}}$  is the portion of the total luminosity that is carried away in the form of radiation. This relatively simple equation is valid only if viscous dissipation can be neglected. The situation becomes much more complex if viscous dissipation is non-negligible; unfortunately, all that is known about the viscous dissipation tensor (eq. 6 in [221]) is that it has a lower bound of zero, which brings about large uncertainties in models with convective cores.

In the case of intermediate- and high-mass main-sequence stars, which do have convective cores, overshooting may lead to a substantial increase in the size of the convective core compared to that predicted by the Ledoux and Schwarzschild criteria, thereby also affecting their predicted lifetimes and evolutionary paths. One must accordingly calibrate the convective overshooting “efficiency” when computing evolutionary models for stars with convective cores. A commonly adopted procedure is to parameterize the convective overshoot in terms of the local pressure scale height  $\lambda_P$  (see, e.g., [67] and references therein). Another, more sophisticated approach has recently been suggested by [272], who provide the following equation that must be solved for the actual extent of the convective core radius  $r_{\text{cc}}$ :

$$\int_0^{r_0} f_{\text{over}} (L_{\text{rad}} - L) \frac{1}{T^2} \frac{dT}{dr} dr + \int_{r_0}^{r_{\text{cc}}} (2 - f_{\text{over}}) (L_{\text{rad}} - L) \frac{1}{T^2} \frac{dT}{dr} dr = 0, \quad (92)$$

where  $r_0$  is the “classical” core boundary (i.e., as given by eq. 64 or 65), and  $f_{\text{over}}$  is a free parameter that is evaluated by comparison with the observations, and which is, in general, a function of mass and chemical composition (see [272] for additional details).

As pointed out by [256], theoretical investigations show that the core-helium burning phase of low-mass stars may be characterized initially by convective core overshooting, and later by the formation of a *semiconvective zone* surrounding the convective core. What happens in this phase is that the opacity of the matter in the convective core becomes higher and higher as He is transformed into C, as a consequence of the increasing contribution of the free-free process with increasing carbon abundance ([51]). Since a chemical composition discontinuity is progressively built up between the C-enriched core and the He-rich envelope, a discontinuity in  $\bar{\kappa}_R$  also results. This, in turn, leads to a discontinuity in the radiative gradient  $\nabla_{\text{rad}}$  across the boundary of the convective core (see eq. 13). Convective overshooting is then assumed to take place, the convective core increasing in size until convective neutrality is restored at its edge. However, once the convective core exceeds a certain size, the radiative gradient reaches a minimum and then increases with increasing distance from the center. According to canonical theory, the end result is the development of a *partially mixed*, convectively neutral (i.e., with  $\nabla_{\text{rad}} = \nabla_{\text{ad}}$ ), “semiconvective” region outside the “canonical” convective core. Exceedingly clear descriptions of the entire process have been provided in [253, 255].

The semiconvective phenomenon has been known for almost 50 years, having first been identified by Schwarzschild & Härm in their study of the evolution of high-mass stars ([235]). In it, they described the occurrence of a zone – the semiconvective zone – just outside the convective core “in which the convection is so slow that it does not contribute to the energy transport but is fast enough to modify the composition, so that convective neutrality is maintained in every layer of this zone.” Naturally, since they were dealing with the convective cores of high-mass MS stars, in their work they only tackled the phenomenon of *hydrogen* semiconvection. In low-mass stars, on the other hand, semiconvection takes place in the core He-burning phase, and may accordingly be termed helium semiconvection. Interestingly, in the former case semiconvection arises because the opacity of the hydrogen-rich matter just outside the convective core is higher than just inside the convective core, whereas the opposite is true for the convective overshooting that leads to semiconvection in HB stars. For yet another example of the occurrence of semiconvection in low-mass stars, the reader is referred to the studies of [143, 144, 130] on the role played by semiconvection on the AGB phase.

By bringing He-rich material into the core, a semiconvective zone enables a low-mass star to burn helium that is present over a much wider range in mass than would otherwise have been possible, thereby leading to a significant increase in the HB lifetime and also dramatically impacting the morphology of HB evolutionary tracks in the HRD (e.g., [51, 52, 84, 212, 256, 260, 261, 211, 255]). From the point of view of a fluid dynamics theoretician, on the other hand, “the still unsolved problem” – in the words of Canuto ([38]) – “is as follows: what are the values of  $\nabla$  and  $\nabla_\mu$  in such a zone?” In addition, canonical theory simply assumes that the composition distribution within the semiconvective zone instantaneously adjusts to insure convective neutrality, without any attempt to follow the time evolution of the convective layer. The reader is referred to [36] for a recent, detailed discussion of this problem, and to [175] for 2D hydrodynamical calculations and comparison of the results with commonly adopted prescriptions for the

treatment of semiconvection in stellar interiors (see also [12]).

An important problem related to the semiconvection mechanism operating in HB stars are the so-called “breathing pulses,” which lead to abrupt *enhancements* in the core helium abundance as a consequence of sudden outward movements of the edge of the convective core when He is approaching exhaustion in the core (i.e., when  $Y_{\text{core}} \lesssim 0.1$ ; e.g., [256, 257, 50, 34, 255]). The main question here is whether these “breathing pulses” are real or instead an artifact of the canonical assumptions used to treat convection and mixing in stellar interiors (e.g., [253, 93, 255]). Since these pulses significantly increase the amount of He fuel that is burnt on the HB phase, they accordingly decrease the amount of He that is available for burning on the AGB phase; therefore, they may crucially affect the predicted number ratios between AGB and HB stars (e.g., [211]). While inclusion of semiconvection is indeed crucial for correctly predicting the observed AGB-to-HB number ratio (e.g., [29, 211, 42]), comparisons between models that allow for the breathing pulses and the observations strongly suggest that these pulses do not occur in real stars (e.g., [43]). However, if time-dependent overshooting is adopted as opposed to canonical semiconvection, breathing pulses arise naturally and the corresponding models are still consistent with the observations ([255]). Indeed, in the HB computations by [255], in which time-dependent overshooting was considered, the overall results (HB lifetime, evolutionary track morphology) were found to be in excellent agreement with those using canonical semiconvection but suppressing breathing pulses, with one important difference: the breathing pulses, by perturbing the interior structure as they redistribute carbon from the central He-burning regions, cause fluctuations in the stellar radius, and thus in the predicted RR Lyrae pulsation periods, which may be related with the – often erratic – period changes observed in RR Lyrae stars ([264, 255]; see also [74] and [188], and §9 in [55] for a review of the available observations). On the other hand, [25] have argued that convective breathing pulses, and in fact even semiconvection itself, are an artifact of the use of a local theory of convection, disappearing when a non-local formalism is properly adopted. However, the model of convection upon which the reasoning by [25] is based has been strongly questioned ([209]). The reader is referred to [86] and [66] for recent discussions on this hotly debated topic.

To close, we note that semiconvection at the base of the convective *envelope* has recently been found in evolved solar models (at an evolutionary age of 6.5 Gyr) by [10], as a consequence of diffusion increasing the abundances of heavier elements (hence the opacity) below the base of the convective zone. (See §6.2.3 in the monograph by [251] for a review of overshooting at the base of the solar convective envelope.) To the best of the present author’s knowledge, a similar phenomenon has not yet been described/included in other studies of low-mass stellar evolution.

### 3.3.3. *Conductive Transport*

Besides radiation and convection, energy can also be transported from one place in the star to another by the movement of individual particles (i.e., electrons, protons, neutrons,  $\alpha$ -particles, etc.). In practice, given their low masses (hence high velocities) and the high

degree of ionization in stellar interiors, only electrons play a truly significant role in this regard.

Still, under normal conditions, it can be shown that energy transport by conduction is much smaller than by either radiation or/and convection, so that it is safe to neglect its contribution when computing stellar structure models. This rule of thumb, however, breaks down under one circumstance which is of crucial importance in the life of a low-mass star, namely, the development of *electron degeneracy*. When matter becomes degenerate – which is what happens in the cores of RGB and AGB stars and in white dwarfs – the low-lying energy states all become filled, which effectively prevents electrons from undergoing frequent collisions with other ions or electrons (since if they did collide their energies might change, which cannot frequently happen since only high-lying energy states have not yet been filled). As a consequence, the mean free path of an electron increases dramatically, and a typical electron may be able to travel a large distance before finally colliding and releasing its excess energy. A strongly degenerate gas is often approximated by a zero-temperature Fermi gas; however, this is not a sufficiently good approximation in the case of low-mass RGB and AGB stars, in which degeneracy is not so strong. Note that, in the evolutionary phases preceding the RGB, the gas in the deep stellar interior can be approximated as a fully ionized perfect gas.

Conductive opacity  $\kappa_c$  is defined in such a way that the energy flux by electron conduction takes on a form similar to that which applies to radiative transport (eq. 34), namely,

$$F_c = -\frac{4ac}{3\kappa_c\rho} T^3 \frac{\partial T}{\partial r}, \quad (93)$$

where  $F_c$  is the conductive energy flux. Therefore, in a region where conduction is important, the total energy flux is given by

$$F = F_{\text{rad}} + F_c = -\frac{4ac}{3\kappa_{\text{equiv}}\rho} T^3 \frac{\partial T}{\partial r}, \quad (94)$$

where the “equivalent opacity”  $\kappa_{\text{equiv}}$  is given by

$$\frac{1}{\kappa_{\text{equiv}}} = \frac{1}{\kappa_R} + \frac{1}{\kappa_c}. \quad (95)$$

As can be seen, the radiative and conductive opacities add as do the resistances of two resistors associated in parallel in a simple electric circuit; this means that energy flow proceeds primarily through the “easier” of the two channels (i.e., the one with the lower opacity), just like electricity will flow primarily through the resistor with the lower resistance. Note that this rule is not valid for the computation of either the radiative or conductive opacities individually; indeed, the former is the result of the summation over many different physical processes, such as bound-bound (or line) transitions, bound-free transitions (photoionization), free-free transitions (inverse bremsstrahlung), molecular transitions, Thomson scattering, etc. (see, e.g., eq. 8.18 in [114]), whereas the latter, according to the so-called *Matthiessen rule*, is also given by the sum of electron-ion and electron-electron contributions (see, e.g., [285]) – though it should be noted that this

rule is, in fact, an approximation which is strictly valid only under conditions of strong electron degeneracy (see [285, 133]).

Over the past several decades, the most frequently adopted recipes for conductive opacities in stellar interior calculations have been those by Hubbard & Lampe ([133]) and by Itoh and co-workers (e.g., [149]). However, and as noted by [56], these recipes are not strictly valid in the interiors of low-mass RGB stars, where matter is in an intermediate form between a gas and a liquid (Coulomb coupling parameter  $\Gamma \lesssim 0.8$ ). The more recent calculations by [192, 193] have likewise not been strictly extended to these intermediate-coupling regimes, though an interpolation scheme was adopted which guarantees a smooth fitting across the crucial region (see Fig. 17 in [55]) between  $\Gamma \rightarrow 0$  and  $\Gamma > 1$ .

More recently, [55] also noted that the available conductive opacity calculations have not taken into due account the fact that the matter in RGB interiors is *not* strongly degenerate, being better characterized instead by intermediate degeneracy levels (see Fig. 18 in [55]). This statement is especially applicable to the electron-electron component, which is of great importance for low-mass RGB interiors in particular (e.g., [56, 55]).

In order to provide conductive opacity calculations that should be more safely applicable to the conditions characterizing the interiors of low-mass RGB stars, [44] have recently undertaken the task of revisiting the work by [192, 193], addressing the limitations that were reviewed in the previous paragraphs and taking into account additional physical processes ([244]) which had not been previously incorporated into such calculations. As a result, [44] came up with revised conductive opacities which differ in some important respects from those provided in previous work for the physical conditions prevailing in the interiors of low-mass RGB stars (see Fig. 4 in their paper), and which present a non-negligible impact on such observables as the luminosity of the RGB tip, the luminosities of HB and RR Lyrae stars, and the predicted RR Lyrae pulsation periods (see [44] for further details). These revised conductive opacities are also available on the web.<sup>6</sup>

### 3.3.4. Some Additional Open Problems

*Radiative opacities:* As already stated (Sec. 3.3.1), great effort has been dedicated, over the past 15 years or so, to compute realistic tabulations of Rosseland mean opacities (and the accompanying EOS) for use in astrophysical applications. These efforts have been mainly led by the OPAL team at the Lawrence Livermore National Laboratory (e.g., [147]; see also footnote 3) and by the OP team, led by M. Seaton at the University College London ([240, 8] and reference therein; see footnote 4). The opacities provided by these two groups have proven of great importance in explaining (and even predicting, as in the case of the EC 14026 non-radial pulsators) a variety of stellar pulsation-related phenomena (e.g., [73, 247, 246, 63, 24, 176] and references therein). In the low-temperature regime, where molecular effects become important, the Alexander-

---

<sup>6</sup> <http://www.ioffe.ru/astro/conduct/index.html>

Ferguson opacities ([1]) are generally to be preferred, but the recent updates and extensions by [98] should now be implemented as well.<sup>7</sup> Account should be taken of possible deviations from scaled-solar abundances, since these may have dramatic impacts on the resulting stellar models (e.g., [279]).

The improved calculations provided by these groups have proved of key importance for the solution of several long-standing problems in stellar astrophysics. Yet, some significant differences between OPAL and OP results still exist, and may reach up to 25% in some key regions of parameter space ([241, 176]), such as the driving regions in some types of pulsating stars (e.g., [151, 176]), leading to significantly different results depending on which set of opacities is used. Some of these differences appear to be due to the different prescriptions for the EOS used in the different projects ([241]). Needless to say, a resolution of the discrepancies that are present both at the radiative opacities and EOS fronts would be crucial to put the models of the structure, evolution, and pulsation of low-mass stars on a firmer footing. In this sense, attention should be called to the recent, provocative work by [268, 269] (and references therein), according to whom improvements in the treatment of several important physical ingredients are still in order.

*Convection beyond the Mixing Length Theory:* As can easily be realized from Sec. 3.3.2, the currently most frequently adopted prescriptions for convection in stellar interiors are rather crude, this remaining, in fact, one of the most important sources of uncertainty in the computation of stellar models. In recent years, some attempts have been made to provide a more realistic description of convection for use in stellar interior calculations, going beyond the extremely simplified (and perhaps simplistic) mixing length formalism. In particular, [40, 41] have developed the so-called *full spectrum of turbulence* model which, unlike the mixing length theory, takes into account the existence of turbulent eddies of all sizes. In this theory, the concept of mixing length is also redefined; in particular, the authors advocate the use of  $\ell \propto z$  in the computation of stellar models, where  $z$  is the distance to the top of the convection zone as determined by the Schwarzschild criterion (eq. 65).

More recently, [39] presented an extension of the original full spectrum of turbulence model, in which the processes that generate the turbulence were more carefully considered. Unfortunately, a free parameter  $\alpha^*$  (namely, a constant of proportionality, presumably smaller than 0.2 in absolute value, between the mixing length and the pressure scale height  $\lambda_P$  at the upper boundary of the convection zone; see eq. [96] in [39]) still has to be adjusted to the data for the Sun in order to “calibrate” this model.

In reality, both the mixing length and the full spectrum of turbulence models face a strong challenge when confronted with both hydrodynamical simulations and the available asteroseismological data for the Sun (see §2.1.3 in [58] for a recent review and additional references). A recent attempt at calibrating the free parameters of both the mixing length and full spectrum of turbulence theories on the basis of 2D hydrodynamical simulations has been provided by [170] (see also [4]). According to their results, the parameter  $\alpha_\ell$  in the former theory presents a variation from  $\sim 1.3$  for F-type dwarfs

---

<sup>7</sup> <http://webs.wichita.edu/physics/opacity/>

to  $\sim 1.75$  for K-type subgiants, there existing a plateau in the neighborhood of the Sun where  $\alpha_\ell$  remains nearly constant. It remains to be seen whether these variations in  $\alpha_\ell$  can be reconciled with the observations of globular cluster stars (e.g., [187, 99]). Also for the full spectrum of turbulence model, [170] find a significant variation in  $\alpha^*$  depending on the spectral type, with absolute values ranging from slightly negative for the cooler stars up to 0.6 for K-type dwarfs (note that, according to [39], such a value should not be larger than 0.2).

In fact, and as also pointed out in [58], the mixing length formalism appears to provide a *better* description of the thermal profile of the solar convective region, as compared with the full spectrum of turbulence model. However, adding to an already confusing situation, [37] has challenged the interpretation of the results of the numerical simulations, pointing out important limitations of 2D (as compared to 3D) calculations and arguing that such simulations in fact rule out the mixing length theory while not being inconsistent with the full spectrum of turbulence model. One way or another, it appears clear that the solution to this problem lies in the computation of realistic 3D hydrodynamical simulations, which may differ substantially from both 2D simulations and the mixing length or full spectrum of turbulence predictions (see [171] for a very recent example).

### 3.4. Thermonuclear Reaction Rates

Thermonuclear reaction rates are of paramount importance for realistic stellar model computations for two main reasons: first, it is the energy generated by these reactions that allows the star to shine during most of its lifetime; second, these reactions lead to dramatic changes in the chemical compositions of (especially) the innermost regions of the stars, which is the primary driver of changes over time in the stellar structure, and accordingly also the reason why stars go through different evolutionary phases in the course of their existence.

In state-of-the-art evolutionary calculations, *nuclear reaction networks* are routinely employed which take into account many different nuclear reactions, thus allowing one to follow the time evolution of a variety of different nuclear species. In the case of low-mass stars, the most important reactions that must be included in such networks are obviously the H- and He-burning reactions, most important among these being the so-called *proton-proton (PP) chain* for main-sequence stars, the *CNO cycle* for RGB, HB, and AGB stars, and the *triple- $\alpha$  process* for the HB and AGB phases. In addition, the  $^{12}\text{C}(\alpha, \gamma)^{16}\text{O}$  reaction becomes increasingly important as a He-burning mechanism towards the end of the HB phase, when He is approaching exhaustion and the triple- $\alpha$  process becomes less frequent (involving, as it does, the almost simultaneous combination of three  $^4\text{He}$  nuclei). Proton-capture nucleosynthesis may also be of considerable importance, particularly in view of observed abundance anomalies (especially among globular cluster stars) in such elements as Na and Al ([112] and references therein). Neutron-capture nucleosynthesis (the so-called slow neutron capture process, or simply *s*-process; see [132] for the first usage of the term in the scientific literature, and [30, 35] for more extensive developments of the idea) may also take place during the AGB phase

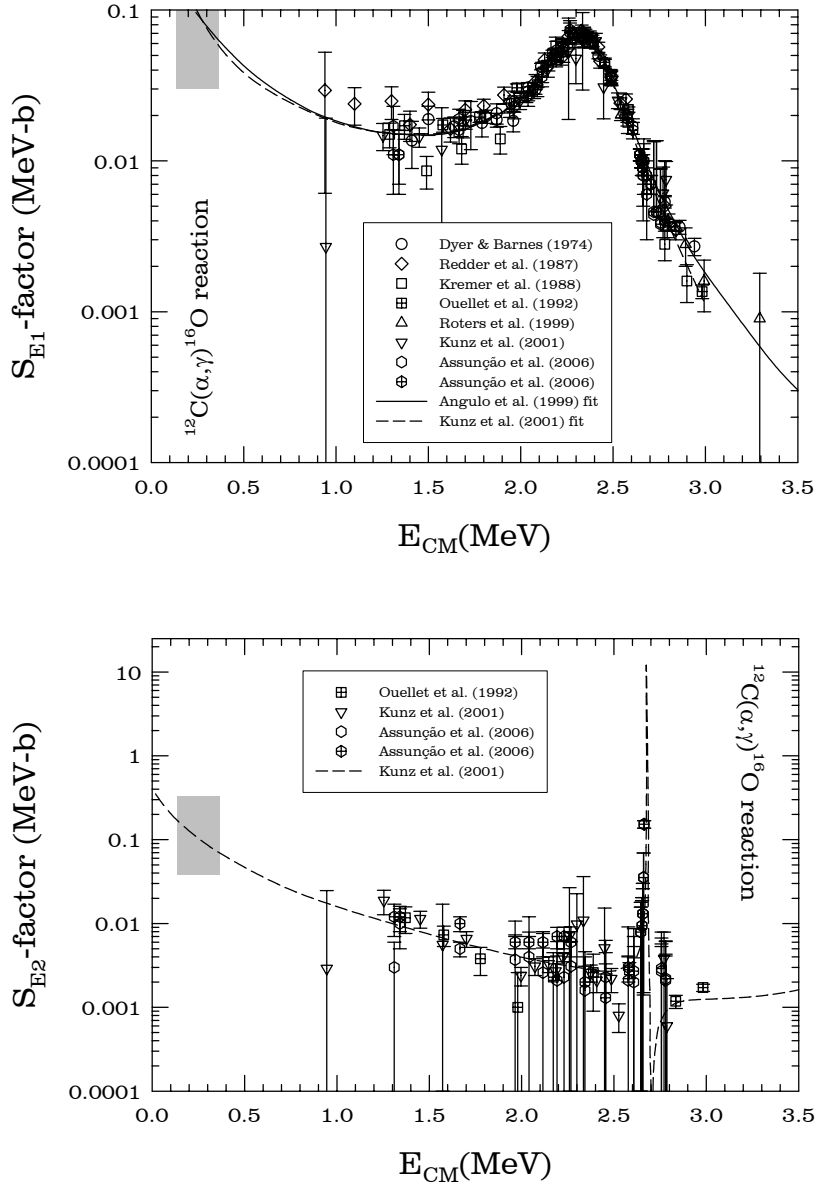


**FIGURE 3.** (top panel) Astrophysical  $S$ -factor (E1 component, in MeV-barn), for the  $^{12}\text{C}(\alpha, \gamma)^{16}\text{O}$  nuclear reaction as a function of the energy in the center-of-mass reference system (in MeV). The sources of the indicated experimental data are shown in the inset. The two different symbols used in the Assunção et al. (2006) case refer to two different solutions proposed by the authors (see their paper for further details). The fits to the data proposed in [3] (solid line) and in [165] (dashed line) are also shown. The region of astrophysical interest, as indicated by the Gamow peak temperature and  $e$ -width at a temperature  $1.35 \times 10^8$  K (a value typical for He-burning at the end of the HB phase), is shown schematically as a gray band. Note that the y-scale is logarithmic. (bottom panel) As in the top panel, but for the E2 component.

of low-mass stars (e.g., [141, 252]), due to the strong neutron fluxes that may be provided by such reactions as  $^{13}\text{C}(\alpha, n)^{16}\text{O}$  and  $^{22}\text{Ne}(\alpha, n)^{25}\text{Mg}$ , particularly in the course of thermal pulses (see §5).

All these reactions and cycles are reviewed in great detail in the monographs by Clayton ([71]) and Rolfs & Rodney ([214]). Modern calculations most frequently adopt the nuclear reaction rates and  $Q$  values that are provided in the NACRE database<sup>8</sup> ([3]), though on occasion computations are also provided which incorporate revised rates for some specific reactions that have been recommended in the nuclear physics literature (for recent examples, see, e.g., [190, 280, 70]); conversely, it frequently happens that, on the basis of astronomical observations and astrophysical considerations, changes to the recommended values for some thermonuclear reaction rates are indicated (e.g., [174, 275] and references therein). In fact, one of the most spectacular astrophysical success stories ever came precisely from an argument of this type: Fred Hoyle and co-workers ([131]) realized that the observed (i.e., fairly high) amount of carbon in the Universe would be completely inconsistent with stellar nucleosynthesis arguments, *unless* the  ${}^8\text{Be}(\alpha, \gamma){}^{12}\text{C}$  reaction proceeded through a (then unknown) *resonance* located very near the  ${}^8\text{Be} + \alpha$  threshold, i.e., at an energy around 7.68 MeV. This reaction forms the second “leg” of the triple- $\alpha$  process, the first being  ${}^4\text{He} + {}^4\text{He} \rightleftharpoons {}^8\text{Be}$  ([183, 226]). The problem with this process, it was argued, is that  ${}^8\text{Be}$  very rapidly decays back into two  $\alpha$  particles, thus making it exceedingly unlikely that substantial amounts of  ${}^{12}\text{C}$  can be formed without a resonance being present close to the  ${}^8\text{Be} + \alpha$  threshold. In addition to the corresponding  ${}^{12}\text{C}$  nuclear energy level proper, Hoyle et al. also predicted the precise quantum-mechanical properties (angular momentum and parity) of the corresponding  ${}^{12}\text{C}$  nuclear energy level. Amazingly, these purely astrophysical predictions were soon verified in laboratory experiments ([72]). Salpeter has recently published a very interesting review paper that describes these and other related developments in nuclear astrophysics from a historical perspective ([228]).

The major uncertainty affecting the application of nuclear reaction rates that are measured in the laboratory to the realm of stellar interiors is the fact that, in the latter, those same reactions usually take place at much lower energies. This is a consequence of the fact that there are so very many particles available in a typical stellar interior that even if a minor fraction of them – i.e., those located towards the high-energy tail of the Maxwell-Boltzmann velocity distribution, or (more precisely) around the so-called “Gamow peak” – are able to actually take part in nuclear reactions, still the required amount of energy to support the star can be generated in the process. The Gamow peak defines, by combining the competing effects of the high-energy tail of the Maxwell-Boltzmann distribution with the probability of tunneling through the corresponding Coulomb barrier, the most effective energy for thermonuclear reactions (see, e.g., §4.3 in [71], or §4.2 in [214]). In the laboratory, on the other hand, at similar energies, it is impractical to follow a sufficient number of events that might stand a chance of revealing even a bare minimum of such reaction events ever taking place. Therefore, in stellar astrophysics work, one is routinely forced to *extrapolate* laboratory measurements of the cross sections towards energies of relevance for stellar interiors (as indicated by the position of the Gamow peak), to rely on theoretical predictions of nuclear physics, and/or to use a combination of these two approaches.  ${}^{12}\text{C}(p, \gamma){}^{13}\text{N}$ , the key reaction that starts the CNO cycle, is a classical example of a non-resonant reaction whose rate is primarily

---

<sup>8</sup> <http://pntpmp.ulb.ac.be/Nacre/>

affected by this type of uncertainty (see, e.g., §6.2.1 in [214]).

Of course, when carrying out such extrapolations, there is always the danger that previously unknown nuclear resonances may fall in the “uncharted territory” frequently represented by astrophysical energies – but this is a risk that must be assumed in stellar structure/evolution work. On the other hand, and as already pointed out, this is also one of the reasons why astrophysics may be used as an empirical probe of nuclear reactions, even beyond the domain within reach in a physicist’s laboratory.

### 3.4.1. The $^{12}\text{C}(\alpha, \gamma)^{16}\text{O}$ Reaction

Probably the main source of uncertainty in the calculation of the structure and evolution of low-mass stars, as far as nuclear reactions rates are concerned, is the  $^{12}\text{C}(\alpha, \gamma)^{16}\text{O}$  reaction – which, as already stated, becomes of increasing importance towards the end of the HB phase. At present, the cross section for this reaction, for typical He-burning temperatures, is 5-6 orders of magnitude below the experimental sensitivity ([164]).

This reaction proceeds through several different channels (see, e.g., Fig. 1 in [164]), the most important of which being called the E1 and E2 channels. In its essence, the E1 channel involves the low-energy tail of the  $^{16}\text{O}$  nuclear energy level that is located 2.418 MeV above the  $^{12}\text{C} + \alpha$  rest mass energy, plus a resonance that is located 45 keV *below* the latter (a so-called *subthreshold* resonance). The E2 channel, in turn, also involves a subthreshold resonance, namely, the one located 245 keV below the  $^{12}\text{C} + \alpha$  rest mass energy, plus the direct-capture process into the  $^{16}\text{O}$  ground level. The fact that more than one resonance is at play in each case leads to *interference effects* between them. As shown in [214] (see their Fig. 7.6), the resulting cross section depends on whether such interference effects are constructive or destructive. While for the E2 channel it is possible to determine the sign of the interference effects from measurements at relatively high energies (maximum interference is expected around 3 MeV), in the case of the E1 channel measurements at energies around 1.4 MeV or lower are also required. From the available experimental data, it appears that constructive interference is at play for both the E1 (see Fig. 7.10 in [214]) and E2 cases (see Fig. 3, and compare with Fig. 7.6, middle panel, in [214]).

To illustrate the present level of uncertainty in evaluating the reaction rate that should be used in stellar applications, in Fig. 3 (*upper panel*) we plot, as an example, some of the available laboratory data for the E1 branch, as compiled on the NACRE team web page, and supplemented by the more recent data from [218, 165, 7]. Here the so-called “astrophysical *S*-factors” are used as opposed to cross sections proper, the latter being obtained in terms of the former using the following expression:

$$\sigma(E) = \frac{S(E)}{E} e^{-2\pi\eta}, \quad (96)$$

where  $E$  is the energy in the center-of-mass system, and  $\eta$  is given by

$$\eta = \frac{Z_1 Z_2 e^2}{\hbar v}, \quad (97)$$

where  $Z_1$  and  $Z_2$  represent the atomic numbers of nuclei 1 and 2, respectively,  $e$  is the electron charge,  $\hbar = h/(2\pi)$  (with  $h$  being the Planck constant), and  $v$  is the relative velocity in the center-of-mass system. The goal here is to factor out the non-nuclear ingredients, such as the geometric de Broglie cross section  $\pi\tilde{\chi}^2 \propto 1/E$  and the probability of tunneling through the Coulomb barrier  $\propto \exp(-2\pi\eta)$ . Therefore,  $S(E)$  is, by design, essentially the “purely nuclear” contribution to the cross section  $\sigma(E)$ .

In Fig. 3 we also show, as a solid line, the (theoretically-motivated) fit to the data proposed by [3], as well as the similar fit more recently advanced by [165]. In addition, the range of energies of interest for low-mass stars, as given by the Gamow peak position and  $e$ -width [from eqs. (4-47) and (4-52) in [71], respectively] at a temperature of  $1.35 \times 10^8$  K (as appropriate for the cores of helium-burning HB stars), is schematically shown as a gray band. While the fits proposed in [3] and [165] are in good agreement in the region of interest, the situation is in fact more complex in the case of the E2 component (see Fig. 3, *bottom panel*), which leads to significant differences between the final recommended  $S$ -factors in [3] and [165] (see Tables 1 and 4 and Fig. 3 in [165]). In this sense, note, from Fig. 3, that the E1 and E2 components have similar magnitudes in the energy range of interest for stellar interiors work. (All additional components, according to the bottom panel in Fig. 1 of [165], are some three orders of magnitude smaller.)

### 3.4.2. Screening Factors

Before closing, we note that, since in the stellar interior the nuclei participating in the nuclear reactions are actually immersed in a plasma, the latter may actually become polarized, with electron “clouds” forming around the positive nuclei and thus leading to some “shielding” of the repulsive Coulomb potential – with the end result that the nuclear reactions proceed at faster rates than in the laboratory. This phenomenon is accounted for using the so-called *plasma screening factors* (see, e.g., §6.8 in [71] for a simple treatment). In modern stellar structure work, screening factors are still most frequently taken from [90, 111]. However, and as previously pointed out in [56], reportedly more accurate prescriptions have been provided by [283] (see their §3). The impact of the Yakovlev-Shalybkov screening factors, to the best of the present author’s knowledge, has unfortunately never been seriously evaluated in the context of the structure and evolution of low-mass stars.

## 3.5. Boundary Conditions

In order to integrate the set of eqs. (1)-(4), in addition to the adequate input physics indicated by eqs. (6)-(10), four suitable boundary conditions are obviously needed. Two of these – the *central boundary conditions* – are self-explanatory, namely (in Lagrangean notation):

$$r(m=0) = 0, \quad L(m=0) = 0. \quad (98)$$

Though simple, these boundary conditions must be used with due care, or else they may lead to a singularity in the star center (see eqs. 1-4, and §3.2 in [223] for a recent discussion).

The other two boundary conditions come from the outer border of the star; basically, one needs to specify how pressure and temperature change with depth close to the stellar surface (defined as the point where the Lagrangean coordinate mass reaches its maximum value, corresponding to the total mass of the star). One cannot simply state the temperature and pressure at the “actual” surface of the star, since built-in into the aforementioned equations is the hypothesis of near isotropy of the radiation field, which breaks down more dramatically the closer one gets to the surface. For this reason, so-called *photospheric boundary conditions* must be used instead, which should ideally be based on detailed model atmospheres which take into account such potentially important effects as non-zero curvature, microturbulence, and deviations from local thermodynamic equilibrium. When such detailed models are lacking or/and practical considerations may prevent them from being implemented, the simpler Eddington boundary condition (see §226 in [96]) is frequently employed.

*Semi-empirical* boundary conditions are also frequently used. In this sense, a still very common approach is to use an analytical relationship between temperature and optical depth  $\tau$  in the atmosphere, as given by Krishna-Swamy ([162]), which reads as follows:

$$T^4 = \frac{3}{4} T_{\text{eff}}^4 \left( \tau + 1.39 - 0.815 e^{-2.54\tau} - 0.025 e^{-30\tau} \right), \quad (99)$$

where  $T_{\text{eff}}$  is the effective temperature. In practice, one assumes this equation to be valid up to a certain optical depth, at which point integration of the stellar interior equations must yield a temperature matching this result.

While for practical reasons the usage of a semi-empirical  $T - \tau$  relation such as eq. (99) may at present be unavoidable (but see [272] for a recent example of evolutionary computations in which actual model atmospheres were used as boundary conditions), one should keep in mind the fundamental limitations of such an approach for the production of realistic stellar models. For instance, eq. (99) is in fact an analytical fit to the data, which however detailed inspection reveals not to be very satisfactory: as can be seen from Fig. 4 (*solid line*), where the same data as used to produce the original Krishna-Swamy fit is shown as star symbols, the fit provided by eq. (99) deviates by up to several hundred Kelvin from the data in the range between  $\tau \simeq 1.5$  and 4, whereas the fit is clearly not steep enough for  $\tau \lesssim 1.0$ . As shown in Fig. 4 (*dashed line*), a much improved fit can be obtained, for  $\tau \leq 2.0$ , with the following expression:

$$T^4 = \frac{3}{4} T_{\text{eff}}^4 \left( \tau + 0.55 - 4.46 \tau^{1.5} + 5.12 \tau^2 - 1.08 \tau^{2.5} \right). \quad (100)$$

In addition, [162] warns against using his scaled-solar expression for stars of spectral types significantly different from solar, and also when convection is efficient as a means of energy transport (as is well known to happen, for instance, in RGB and AGB stars). The  $T - \tau$  relation for the solar atmosphere and for stars of different spectral types is also discussed in §9 of [114].

While the usage of model atmosphere boundary conditions should represent a better approach than relying on such  $T - \tau$  relations, [224], [46], and [272] have indicated that

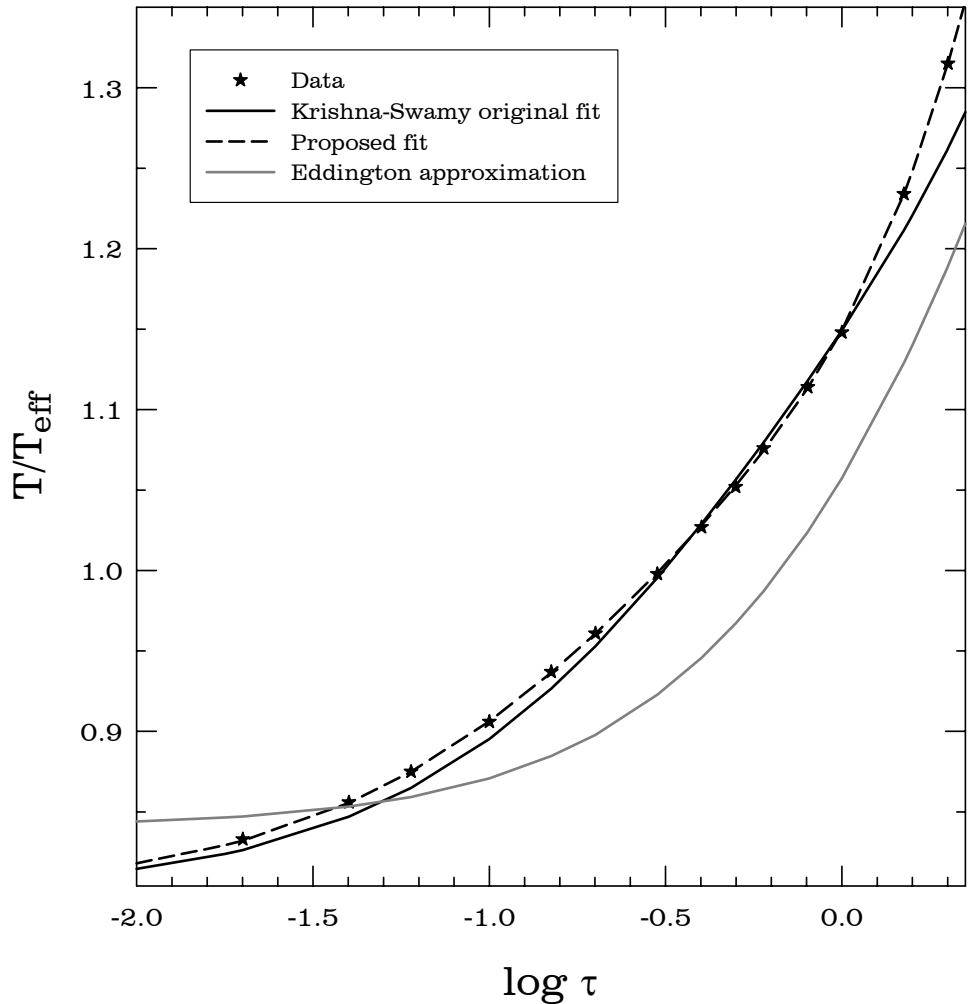


**FIGURE 4.** The data originally used in [162] to derive the frequently employed  $T - \tau$  relation (star symbols) are compared with the original Krishna-Swamy fit (eq. 99, *black solid line*) and the new proposed fit (eq. 100, *dashed line*). As can be clearly seen, the new fit represents a significant improvement over the originally suggested one. Also shown is the resulting  $T - \tau$  relation in the Eddington approximation case (*gray solid line*).

major differences do not surface when comparing the results of stellar models computed with the Krishna-Swamy  $T - \tau$  relation and with actual model atmospheres. However, the latter should be sufficiently detailed that the real physical conditions prevailing in stellar envelopes are reproduced; for instance, Fig. 4 reveals that the simple Eddington approximation already deviates significantly from the semi-empirical  $T - \tau$  relations discussed above.

Some readers may ask, “why not compute the model atmosphere *along* with the interior structure?” While this would be ideal in principle, there is a practical limitation that makes this increasingly prohibitive as the surface is approached. Specifically, when studying the theory of stellar atmospheres (see, e.g., [76, 123]), one finds that the gradient of the radiation pressure is given by

$$\frac{dP_R}{dr} = -\frac{\kappa_{at}\rho}{c} \frac{L}{4\pi r^2}, \quad (101)$$

where  $\kappa_{at}$  is a *flux-weighted opacity* that must be computed from

$$\kappa_{at} \equiv \frac{1}{F} \int_0^\infty \kappa_v F_v dv, \quad (102)$$

with  $F_v$  being the monochromatic flux and  $F$  the integrated net flux. What should be noted here is that  $\kappa_{at}$ , as given by this equation, is *not* the same as the Rosseland mean opacity  $\overline{\kappa_R}$  (eq. 14). While  $\kappa_{at}$  does converge to  $\overline{\kappa_R}$  for large optical depths (see eq. 8.9 in [76]), this is not the case close to the surface of the star. Computing the flux-weighted opacity using eq. (102) represents a formidable challenge, since one must know the radiation field *before* performing the calculations, in addition to having all the relevant *monochromatic* opacity sources built into the code. Unfortunately, this does not look like a realistic approach in the foreseeable future.

### 3.6. Numerical Techniques for the Integration of the Equations

Once all physical ingredients have been properly taken into account, one must choose a numerical technique to carry out the integration of the aforementioned equations describing the structure and evolution of a star. Two of the most frequently used techniques – the *integration of fitting method* (e.g., [234]) and the *relaxation* or *Henyey method* ([127]; see also [135]) – have been described in great detail in [234, 71, 155]. In the former method, the differential equations are independently integrated from the inside of the star out, on the one hand, and from the outside in, on the other – and the solutions are required to match at some intermediate point in the stellar interior. One problem with this method is that these integrations become extremely sensitive to the starting values once stars evolve off the MS (e.g., [239]). As a consequence, in modern work, the Henyey method is by far the most frequently used method.

Whereas the aforementioned works by [71, 155] should be consulted for more details, the overall flavor of the Henyey method can be described as follows. First, one divides the star into discrete mesh points, then replaces the basic differential equations (1)-(4) with difference equations. Given an approximate solution for these difference equations, which can come either from a good guess or more commonly from the previous model in the evolutionary sequence, one then linearizes the difference equations to first order in the corrections and solves the resulting set of linear equations for the corrections, which are then added to the approximate solution to obtain an improved solution. This process is then repeated until the corrections become sufficiently small, i.e., the model converges. In its essence, the Henyey method is basically a glorified version of the Newton-Raphson method for solving equations given an approximate solution. Implementations of the Henyey method are provided in the CD that accompanies the [123] monograph.

In stellar evolution work, one is obviously interested in determining the *time evolution* of the models thus computed. Naturally, one must specify a sufficiently small but finite time step to adopt in the numerical computations. Such a time step can be obtained by

requiring that the change in the abundance of the elements (eq. 12), from one model in the sequence to the next, be sufficiently small. However, some evolutionary phases of low-mass stars, such as the RGB and AGB, present some particular difficulties that prevent such a simple procedure to be applied in practice. In particular, during these phases one often encounters exceedingly narrow H-burning shells, with masses of order  $10^{-3} M_{\odot}$ . Consider one such H-burning shell, whose mass coordinate, in the case of an RGB star, is evolving outward in time. Clearly, even a small outward movement of this shell produces a large change in the hydrogen abundance, since the hydrogen content above the shell is still high, while that underneath it is essentially zero. In terms of the simple method just described, then, the time step required to follow the time evolution of this RGB star becomes very small, thus requiring an enormous number of models, and therefore large amounts of computer time, in order to reliably follow the evolution of the star during its ascent up the RGB ([136]). For this reason, a special technique has been specifically devised and is commonly adopted to treat the time evolution of this evolutionary phase. This is the so-called *shell-shifting* technique, which is described in detail in [124, 137, 216, 271, 254].

In like vein, the helium “flash” phase which follows the end of the RGB phase but precedes the HB is commonly not followed in detail in the course of hydrostatic evolutionary computations (but see [27, 166] for impressive exceptions to this rule). Instead, one commonly applies methods designed to “transport” or “scale” an initial model (taken from the RGB tip) to the zero-age HB phase. Different techniques to accomplish this have recently been reviewed by [242], to which the reader is referred for a comparison of the differences that may result between these approximate techniques and actual evolutionary computations carried out through the He flash.

### 3.7. Comparison with the Observations

Once a theoretical stellar model has been successfully computed, the main output of the code that is of interest to observers (for a star of a given mass and chemical composition) consists in the total luminosity  $L$  and effective temperature  $T_{\text{eff}}$ . Photometric observations, on the other hand, do not yield directly either of these quantities; instead, one is presented with magnitudes (which are converted into *absolute* magnitudes once the interstellar extinction and distance are known) and *color indices*. To compare theoretical predictions with the observations, one again needs to resort to model atmospheres, from which are computed *bolometric corrections* and *color-temperature relations*. While it is common practice to use such relationships derived with a solar-scaled mix of the elements, it is well known that stars pertaining to different stellar populations may present very different proportions of different types of elements, such as (and especially) the  $\alpha$ -capture elements (e.g., [281, 194, 64, 210, 286] and references therein). It has recently been shown ([46]) that model atmospheres computed with the appropriate element abundances may yield appreciably different bolometric corrections and color transformations than scaled-solar ones, with a potentially significant impact on the comparison between model predictions and the observations.

## 4. NON-CANONICAL EFFECTS

The set of equations in §3.1 is strictly valid only in the so-called “standard” or “canonical” scenario, which remains by far the most frequently adopted scenario in the modern stellar astrophysics literature. More specifically, in the canonical framework one ignores any deviations from spherical symmetry, rotation, element diffusion, magnetic fields, and the possible presence of close companions, and each and any of the possible associated instabilities. Active work on each of these specific areas continues to be carried out, but so far a complete evolutionary sequence for a star consistently taking into account all of these neglected effects has not been produced – and, we suspect, is unlikely to be produced in the near future, either. The following describes some of the recent work on some of these topics:

*3D Calculations:* Interesting results of 3D calculations for selected evolutionary phases, especially those where hydrodynamical effects are expected to be more important [i.e., when the acceleration term that appears in eq. (2) outside hydrostatic equilibrium conditions cannot be safely neglected], such as the helium flash at the end of RGB evolution, have recently been presented ([79]). Encouragingly for the standard stellar evolution framework, the final He-burning structures resulting from these calculations are not very different from the 1D model predictions. Likewise, 3D hydrodynamical calculations appear important to properly describe the evolutionary stages preceding the zero-age main sequence phase ([282]), and (as already stated; see §3.3.2 above) have even been claimed ([97]) to provide the key to solve the problem of the observed abundances of  ${}^3\text{He}$  in low-mass stars.

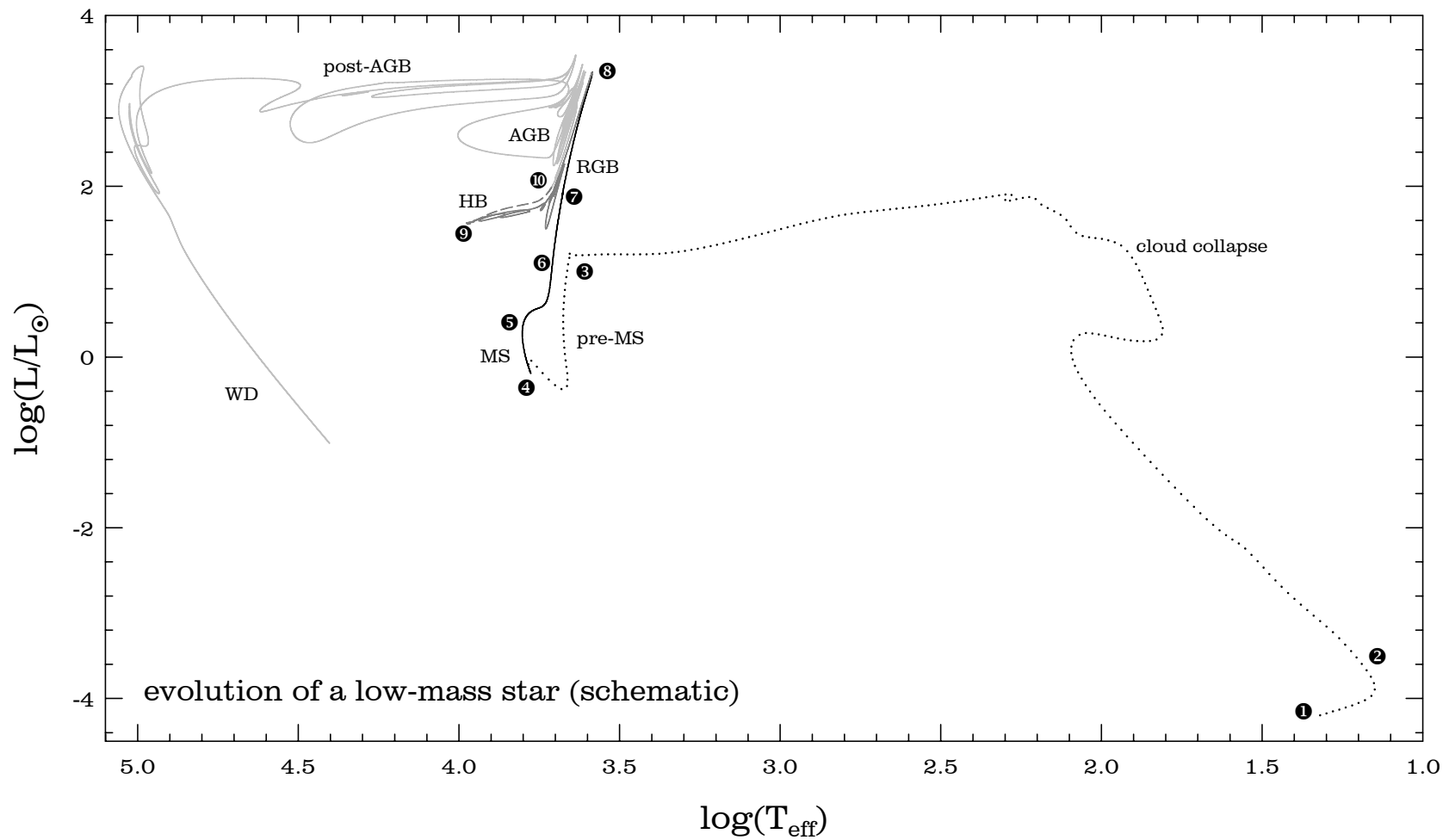
For model stellar atmospheres, 3D calculations have also recently been suggested to be of great importance, leading to fundamental changes in quantities such as the chemical composition that are derived from spectral observations of low-mass stars such as the Sun ([5] and references therein). On the other hand, the revised chemical abundances suggested in these 3D studies lead to solar models which appear to be completely inconsistent with the results of helioseismology (e.g., [11, 13]; see also [119] for a review and additional references), which are in much better agreement with calculations based on the previously accepted solar abundances ([116]). This is one of the most important problems in stellar structure and evolution at present, and its solution may impact several different areas of astrophysics, considering that the “solar metallicity” is a fundamental point of reference in many different astrophysical contexts.

*Rotation:* The impact of rotation is one of the major question marks in the study of the evolution of low-mass stars. Observations of evolved low-mass stars, particularly on the HB phase, reveal a rich phenomenology which is very difficult to explain on the basis of simple models (see [55] for a recent review and references). An illuminating description of some of the fundamental problems encountered in treating angular momentum transport and evolution in rotating low-mass stars is provided in [245], whereas [55] contains examples of several circumstances under which rotation can play a role in interpreting the observed properties of evolved stars in low-mass stellar systems.

*Extra Mixing and Pollution:* As is well known, rotation may also induce extra mixing beyond what is predicted in the canonical framework, which may be crucial in explaining the observed abundance patterns for the light elements in low-mass red giants (e.g., [263, 284, 60, 82, 62, 85, 91, 89, 23, 186]). Such extra mixing may not always be due to rotation: tidal effects due to the presence of close companions may also play an important role in at least some cases ([88, 87]).

In regard to abundance inhomogeneities in globular cluster stars, it is becoming increasingly clear that a fraction of the stars in at least some globular clusters forms from gas that has somehow become contaminated by helium-enriched material in the cluster’s early history, leading to distinct signatures in the observed CMD’s (e.g., [180, 14, 77, 169, 191, 33, 276]). However, it remains far from clear how the large pollution levels that are inferred from these CMD’s can come about, though several different scenarios have been recently advanced for the origin of these (presumably) second-generation stars (e.g., [152, 15, 215, 68] and references therein). As an alternative to this second-generation/pollution scenario, it has also been suggested that protocluster clouds may, as a consequence of diffusion, show important helium abundance variations from one place to the next [243, 69]. One way or another, the confirmation of significant abundance inhomogeneities in at least some globular clusters has weakened somewhat the traditional view that globular star clusters are the closest approximation to a physicist’s laboratory in astronomy ([177]), a view which is generally held due to the great uniformity in their stars’ ages, distances, and (as had been previously thought) chemical composition.

*Mass Loss:* One of the most fundamental, yet least studied, non-canonical ingredients in the evolution of low-mass stars is mass loss. It has long been known that low-mass RGB stars must lose substantial amounts of mass before helium ignition in their cores (e.g., [53, 146, 217, 48, 78]), but no fundamental theory exists that allows one to compute such mass loss from first principles. While mass loss does not affect the evolutionary path of an RGB star in the CMD in a substantial way unless mass loss is so substantial that the star may either directly become a helium WD or ignite helium on its way to the WD cooling curve (e.g., [48, 27, 47, 166, 49]), mass loss does have a huge impact on the subsequent evolution, determining the temperature distribution along the HB (and therefore playing a key role within the framework of the so-called “second parameter” phenomenon that affects the HB morphology of Galactic globular clusters; see, e.g., [55] and references therein) and the ultimate fate of the star. As to the latter, depending on the total mass loss on the RGB phase, the star can go through an AGB manqu , a post-early-AGB, or a post-AGB phase, before finally evolving to the carbon-oxygen WD cooling curve (see, e.g., [94]). Last but not least, there exist several different semi-empirical mass loss formulae that purport to describe the mass loss rates as a function of a star’s physical parameters (such as radius  $R$ , surface gravity  $g$ , and luminosity  $L$ ), none of which being clearly superior to the others in terms of describing the available data; what is worse, the different formulae predict different amounts of mass loss on the RGB, which makes it virtually impossible to predict with any degree of confidence the temperature that the star will have once it reaches the zero-age HB ([54]; see §5 in [55] for a recent review and references). Mass loss may also be a relevant ingredient on the



5: Evolution of a low-mass star in the HRD. All of the main evolutionary phases are shown, from its birth during the cloud collapse and pre-MS phase (*dotted line*) to its death along the WD cooling curve (hot end of the *light gray curve*). The *solid black line* indicates the MS and RGB phases, the *dark gray line* the pre-HB phase, the *dashed line* the HB phase, and the *light gray line* the AGB, post-AGB, and WD phases. The numbers alongside the evolutionary track indicate noteworthy episodes in the life of the star, as discussed in §5. (The pre-MS and cloud collapse phases are adapted from [282], whereas the evolution from the ZAMS onwards has been kindly provided by A. V. Sweigart.)

HB phase proper, at least as far as the derivation of surface gravities from the observed hydrogen line profiles is concerned ([277]).

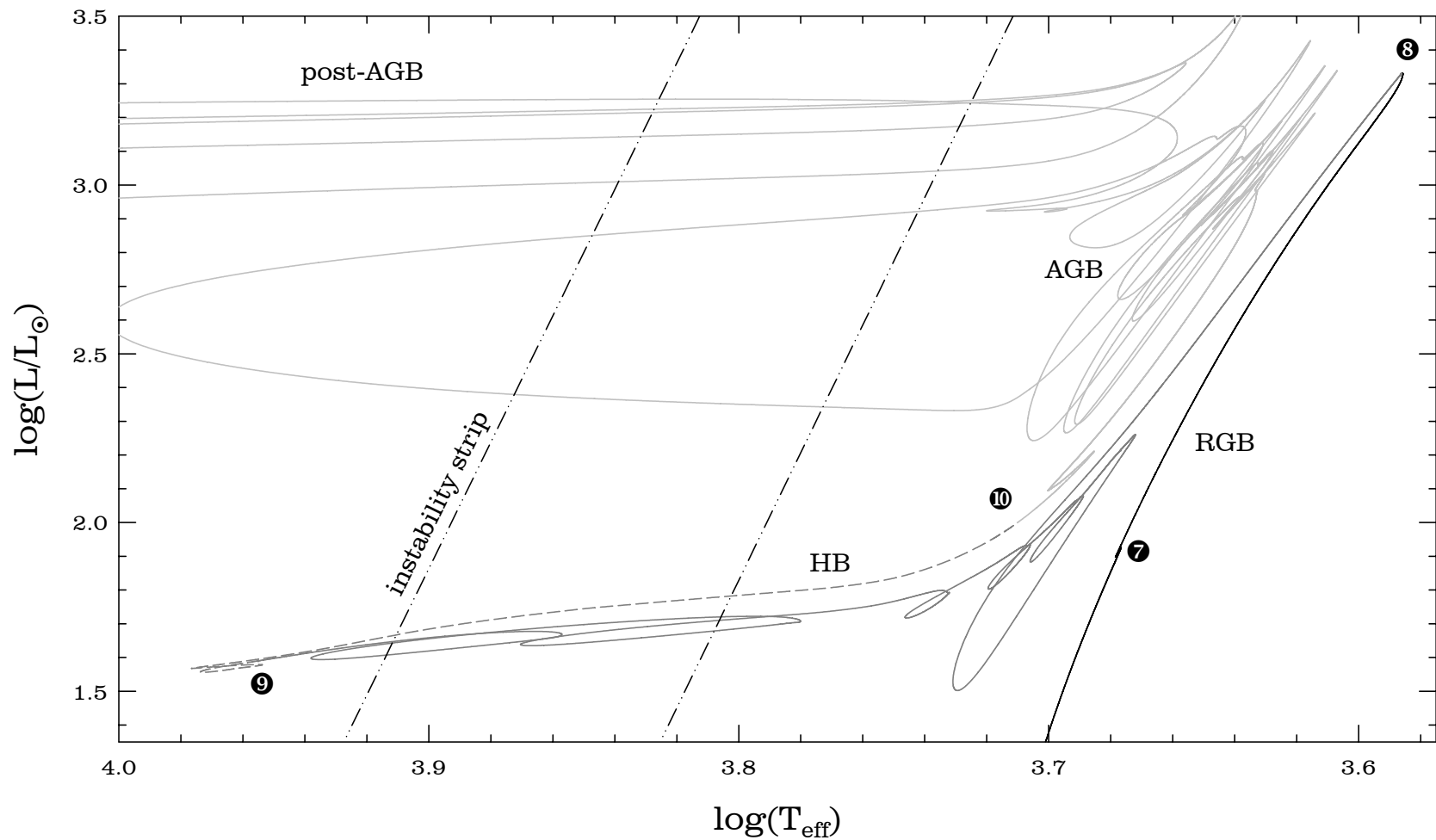
## 5. THE EVOLUTION OF A LOW-MASS STAR: AN OVERVIEW

Now that we have built the fundamental equations of stellar structure and evolution, let us see briefly what has been found to happen, in the case of a low-mass star, when these equations are integrated numerically and the solution is allowed to evolve with time.

In Fig. 5, we show the complete evolutionary path for one such star. The part of the track labeled “cloud collapse” is in fact not the result of hydrostatic calculations as have been primarily discussed in this paper, but rather represents the results of the hydrodynamical simulations performed by [282]. All the other evolutionary phases, in turn, were kindly computed by A. V. Sweigart (2007, *priv. comm.*), using his 1D hydrostatic code. Note that a small, arbitrary shift (in both temperature and luminosity) has been applied to the [282] track, in order to ensure a match with the Sweigart zero-age main sequence (ZAMS).

We now provide a brief summary of the main aspects of the indicated evolution. More detailed discussions can be found in [282] and [21] (cloud collapse phase), [135] and [126] (hydrostatic contraction to the ZAMS), in several papers by Icko Iben, Jr. and collaborators (evolution on the MS and beyond; [137, 146, 141, 142]), and also in several monographs (e.g., [71, 223], etc.). Empirical tests of low-mass stellar evolution using the CMD’s of globular clusters are described in great detail in the review paper by [211]. We follow key phases of the evolution of the (proto-)star according to the numbers that are indicated along specified sections of the evolutionary track in Figs. 5 and 6:

- ❶ We begin by considering a molecular cloud that becomes unstable according to the Jeans ([150]) criterion, and which accordingly collapses and fragments in the process (see [21] for a review). Under normal conditions, some of these fragments – most, as a matter of fact – will eventually give rise to low-mass stars. At this early phase (i.e., prior to ❶), however, the temperature of the fragment is still very low, of order 10 K, and it cannot rise much because the cloud is still optically thin. Accordingly, this phase – not shown in Fig. 5 – is known as the *isothermal phase* of the cloud collapse. Eventually the opacity will increase and the cloud will become optically thick, thus departing from isothermality. When this happens, the proto-star has reached point ❶ in Fig. 5, and the classical “adiabatic phase” commences. According to the calculations provided in [282], it takes the proto-star of order  $1.5 \times 10^5$  yr to reach this point.
- ❷ Around this point a hydrostatic core forms for the first time, and the main accretion phase starts. As can be seen, the luminosity and temperature increase steadily, and the irregularities that are seen in the evolutionary track reflect random fluctuations in the mass accretion rate.
- ❸ When accretion tapers off and the final mass is approached, the photosphere of the proto-star finally becomes visible, the structure becomes fully convective, and its luminosity decreases at almost constant temperature, leading to the vertical segment of evolutionary track – the so-called *Hayashi track* (representing the



6: As in Fig. 5, but zooming in around the HB/upper RGB/AGB phases. The schematic location of the classic instability strip is shown as dot-dashed lines.

canonical pre-MS phase) – shown in Fig. 5. Along most of this vertical segment, the proto-star is fully convective, and the core gets sufficiently hot that deuterium is burnt efficiently. A radiative core only forms at the bottom of the curve, due to the fact that the increasing core temperature also leads to increased ionization and hence to a decrease in the opacity, which as we have seen tends to quench convection (recall eqs. 65 and 38). After this point, the proto-star becomes hotter and increases again in brightness while it is still shrinking in size. The increasing core temperatures also lead to incomplete CNO processing along the first steps of the CN-branch of the CNO cycle, with  $^{12}\text{C}$  in particular being progressively consumed in the core. (For even lower-mass stars, the core temperature never becomes high enough for  $^{12}\text{C}$  to be processed, and the pre-MS evolution remains vertical all the way to the ZAMS.) Until  $^{12}\text{C}$  is finally exhausted in the core and the PPI chain finally begins to operate in equilibrium, with the star settling on the ZAMS, an additional  $5 \times 10^7$  yr will have passed ([135]).

- ④ This is the ZAMS proper. When the star finally settles here, it stops contracting and now evolves along the much longer *nuclear timescale*, which is of order  $10^{10}$  yr for low-mass stars. Accordingly, the star changes position along this region of the HRD only very slowly, with its temperature and luminosity slightly increasing with time as hydrogen is steadily transformed into helium by means of the PP chain (the CNO cycle is currently responsible for a mere 1.5% of the Sun’s current luminosity; see [10]). The MS phase is so slow that the Sun’s radius had already attained about 87% of its current value, its effective temperature was around 97% of the current temperature, and its luminosity some 68% of the current luminosity when the Sun first reached the ZAMS ([10]), which happened some  $4.57 \times 10^9$  yr ago ([9, 251]). A very nice pie chart illustrating the run of several physical quantities with radius for a low-mass ZAMS star is provided in Fig. 7 of [140].
- ⑤ This is the so-called *turn-off point*, which is related to (though not necessarily identical with) the exhaustion of hydrogen in the center of the star. From this point onwards, hydrogen burning ceases to be a central process, becoming instead a *shell-burning* process. Initially, hydrogen burns in a thick shell, whereas the helium-rich core, which is now becoming isothermal, keeps growing in size as a consequence of the helium that is being produced at its outer border. The core cannot grow indefinitely, however: there is a limit to the mass that can exist in an isothermal core and still support the overlying layers, given by the so-called *Schönberg-Chandrasekhar mass* ([231]), or around 10% of the total mass of the star. When its mass increases beyond this point, the core must collapse on a thermal timescale, thus heating up and releasing energy in the process. The rise in core temperatures also leads to a rise in temperature at the base of the thickening H-burning shell, and accordingly H-burning by the CNO cycle becomes increasingly important (having in fact become dominant in the center even before the TO point was reached). As a consequence of the fact that the CNO cycle has a very high temperature dependence, the H-burning shell becomes thinner and thinner. However, not all the energy released by the H-burning shell actually reaches the surface: part of it is used to expand the star’s envelope. As a consequence of this expansion, the star begins to cool down, and the characteristic evolution to the

right constitutes the so-called *subgiant phase*. (In higher-mass stars, this phase proceeds much faster, and gives rise to the so-called *Hertzsprung gap* in the color-magnitude diagram.) The corresponding cooling of the outer layers leads to the formation of a convective envelope, and the star eventually reaches the base of the RGB. The further contraction of the core, moreover, leads to the establishment of electron degeneracy there. Therefore, when the star reaches the base of the RGB, its structure is characterized by a growing but inert, partially degenerate He-core, surrounded by a H-burning shell that is becoming progressively thinner, and an outer convective envelope that is becoming progressively thicker.

- ❶ At this point, the convective envelope reaches its maximum inward penetration, thus leading to the dredge up of material that has been partially processed nuclearly, including a small amount of He. This is the so-called *first dredge-up* phase ([134]). From this point in time onwards, the convective envelope begins to retreat. It takes the star an additional  $10^9$  yr to go from the turn-off point ❸ to this evolutionary stage, whereas the remainder of the RGB phase lasts of order  $10^8$  yr, becoming progressively quicker as higher and higher luminosities are attained.
- ❷ The H-burning shell continues to advance outward in mass, thus leading to a continued increase in mass of the He core. At the indicated point, the H-burning shell actually encounters the chemical composition discontinuity that was left behind as a consequence of the maximum inward penetration of the convective envelope. Since the envelope is naturally H-rich, this means that the H-burning shell is suddenly presented with an extra supply of fuel. The structure of the star, presented with this extra fuel supply, readjusts momentarily to this new situation, with an actual (small) reversal in its direction of evolution before it resumes its ascent of the RGB. The details of this process depend crucially on the precise abundance profile in the H-burning shell (see, e.g., [45]). In the observed CMD's and RGB luminosity functions of globular star clusters, and as first predicted by [267, 139], one in fact identifies the so-called *RGB “bump”* as an observed counterpart of this stellar interior phenomenon (e.g., [154, 103]). Importantly, the RGB bump also appears to correspond to the position in the CMD that marks the onset of mixing of nuclearly-processed elements beyond that predicted by the canonical theory (e.g., [113, 89, 61, 206] and references therein).
- ❸ The final stages of the star's ascent of the RGB are again characterized by the increasing size of the He-core, which keeps on contracting and heating up. Very instructive pie charts showing schematically the structure of the envelope and core of such an RGB star have been provided, respectively, in Figs. 8 and 9 of [140]. At this stage large amounts of energy are lost in the form of neutrinos, such emission being most efficient where the matter is denser – which leads to an actual temperature *inversion* in the core ([267, 138, 216, 262]), its hottest regions moving as far away from the center as  $\sim 0.25 M_\odot$  by the time the RGB tip is reached. As a consequence, when temperatures finally become high enough for the helium-burning reactions to commence, this happens not in the actual center of the star, but in fact in a *shell* inside the He-rich core. In this sense, the fact that the matter in the core is degenerate leads to a dramatic phenomenon which had not been previously encountered in the life of the star – the so-called helium “*flash*”.

To understand the physics behind the flash phenomenon (see [236]), consider first what happens in the case of thermonuclear burning under *non-degenerate* conditions. In this case, the energy input to the medium by the nuclear reactions tends to increase the local temperature, but this temperature increase also tends to increase the local pressure, which in turn tends to expand the region where the reaction is taking place and hence cool down the material, thereby preventing a further increase in the nuclear reaction rate. In other words, thermonuclear burning, under non-degenerate conditions, is a self-regulating process, which allows nuclear burning to proceed quiescently over long periods of time. In the case of degenerate matter, on the other hand, this is not possible: since in this case the EOS lacks a temperature dependence, the local temperature increase does *not* lead to an increase in the local pressure, and therefore the region where burning has started cannot expand and cool down. As a consequence, the energy input by the nuclear reactions leads to an increase in the local temperature, which leads to a further increase in the thermonuclear reaction rates, which leads to another increase in the local temperature, and so on and so forth – giving rise to a so-called *thermonuclear runaway* (hence the term “He flash”), which can only cease once degeneracy is lifted. As a matter of fact, most of the energy that is produced during the He flash (which can exceed, according to [236],  $10^{12} L_\odot$ ; in fact, the models shown in Figs. 5 and 6 reach a peak He-burning luminosity of  $9.2 \times 10^9 L_\odot$ , which should be compared with the luminosity emitted by the entire Galaxy,  $\sim 10^{10} L_\odot$ ) is used to lift up the degeneracy in the core, so that the luminosity of the star does not increase during this so-called “pre-HB phase” – rather the opposite, in fact (see Fig. 6). In addition, since (as already stated) the initial flash occurs off-center, additional flash events take place increasingly closer to the center of the star, until degeneracy has been lifted throughout the He core ([173, 255]). When this happens and the star is finally able to burn helium quiescently in a convective core and hydrogen in a shell, the star has reached the so-called zero-age HB (ZAHB). From the RGB tip to the ZAHB,  $\sim 10^6 – 10^7$  yr will have passed, and around 5% of the core’s helium fuel will have been consumed ([255]). For this reason, only a very small number of stars is expected to be found in the pre-HB evolutionary phase, which is the reason why no such star has ever been positively identified. Very recently, it has been suggested that, as a consequence of the fact that many pre-HB stars are expected to cross the instability strip before they arrive on the ZAHB, some stars which might be going through this phase could be identified as variable stars with peculiarly fast period change rates ([55]), since their periods should depend, according to the period-mean density relation of pulsation theory, on their luminosities and radii, which are both changing on a very short timescale compared with other variables (such as the RR Lyrae and type II Cepheids) which occupy a similar region of the HRD.

⑨ This is the ZAHB that was alluded to in the previous paragraph, marking the onset of the He-burning phase proper – which, in the case of low-mass stars, is referred to as the *horizontal branch* (HB) phase, due to the fact that HB stars all have very nearly the same luminosity irrespective of mass, thus leading to the characteristic horizontal feature that is seen in the CMD’s of globular clusters. HB stars play a particularly important role in determining the distances and ages of old stellar

populations, and also in the interpretation of the formation and evolution history of the Galaxy and its neighboring satellites (see [55] for a recent review). Pie charts illustrating the run of several physical quantities with radius for a ZAHB star located close to the blue edge of the instability strip are provided in Figs. 10 and 11 of [140].

Unfortunately, the exact ZAHB temperature of a star cannot be predicted *a priori*, depending as it does on how much mass the star may have lost on its ascent of the RGB (see the end of §4 for a discussion of some of the problems encountered in treating mass loss in red giant stars). In general, the stars that lose the least amount of mass will fall on the red portion of the ZAHB, whereas those that lose a substantial fraction of their masses will actually fall on the blue ZAHB, some possibly becoming “extreme” HB (EHB) or blue subdwarf (sdB) stars. In turn, intermediate amounts of mass loss should lead to RR Lyrae variable stars, since the classical instability strip actually crosses the HB at intermediate temperatures, as can be inferred from Fig. 6. Of course, not only stars whose ZAHB positions fall within the instability strip will become RR Lyrae variables: in fact, as a consequence of evolution away from the ZAHB, stars which arrived on the blue ZAHB are expected to become RR Lyrae stars later in their lives, when they are already well on their way to become AGB stars (which is precisely what happens with the particular star whose evolutionary path is shown in Fig. 6). Conversely, some stars whose ZAHB position falls on the red HB may also, depending (among other things) on the relative efficiency of their H-burning shells compared with their He-burning cores, develop blueward loops that may take them through the instability strip at some point in the course of their lifetimes.

⑩ When the star reaches this point, which happens  $\sim 10^8$  yr after its arrival on the ZAHB, He has been exhausted in its center, and the star begins its life as a low-mass AGB star. A glimpse at Fig. 6 will promptly reveal that the term “asymptotic” comes from the fact that, for low-mass stars, the evolution proceeds ever closer to the first-ascent RGB, but never quite reaching it. In terms of its internal structure, an AGB star is defined as a star with an inert core (comprised mostly of carbon and oxygen) which burns He in a shell and H in another shell further out, such shells becoming progressively thinner as the star climbs up the AGB. A very instructive diagram comparing the run with radius of several different physical quantities for an HB and an AGB star is provided in Fig. 4 of [146].

In AGB stars, the He- and H-burning shells take turns as the most efficient energy sources, as a consequence of the thermal instabilities that were first encountered in the computations by [237]. In spite of being reminiscent of the He flashes that were found under degenerate conditions at the RGB tip and on the pre-HB phase, electron degeneracy does not play an important role in the case of these so-called “AGB thermal pulses,” the cause here being instead a highly temperature-dependent nuclear energy source operating in a very thin shell ([237]). Stars that have not yet reached this thermally pulsing phase are termed “early AGB” or E-AGB stars ([145]), whereas the thermally pulsing ones, which are preferentially found towards the brighter portions of the AGB, are called, not surprisingly, TP-AGB stars.

In E-AGB stars, the H-burning shell has very little efficiency, since the onset of He burning in a shell has caused the H-burning shell to expand and cool. The onset of He-shell burning causes a temporary reversal in the star's evolutionary direction (as can be seen immediately after point ⑩ in the evolutionary track shown in Fig. 6), which leads to the so-called *AGB clump* in the observed CMD's of well-populated globular clusters and old Local Group galaxies (e.g., [195, 104, 43]). Since the H-burning shell is inefficient, the mass of the He-rich region outside the C-O core cannot increase much in mass during this phase. Eventually, the outward-moving He-burning shell reaches the associated He/H chemical composition discontinuity. When this happens, the He-burning shell dies down, and accordingly the overlying H-burning shell contracts rapidly and is re-ignited. The corresponding He ashes are then compressed and heated, and finally ignite once they reach a critical value (of order  $10^{-3} M_{\odot}$  for a  $0.8 M_{\odot}$  C-O core; see [223]). This marks the onset of the TP-AGB phase.

Unlike what happened in the case of the earlier He flash at the tip of the RGB, matter in this case is *not* degenerate, so that the energy that is liberated in a pulse does lead to an increase in the local pressure, and therefore to an expansion. This expansion cools down the region where He burning is taking place, thus lowering its rate and leading to a phase of quiescent He burning. The H-burning shell, during this expansion phase, is pushed outward to such low temperatures that H burning again dies down. During this quiescent He-burning phase, the He-burning shell consumes all the He that was created by the previous phase of H burning in a shell, until a He/H discontinuity region is again reached. As before, He burning is then again quenched, H burning resumes, and the same processes that had previously given rise to a thermal pulse are again triggered.

Besides nucleosynthetic signatures in the form of *s*-process elements (see §3.3.4), these thermal pulses can give rise to characteristic “loops” in the CMD, such as the ones that can be seen in Fig. 6 (see, e.g., [238, 107, 232, 141]). During some of these loops, the star may again cross the instability strip, becoming a type II Cepheid ([238, 108]). The details of the AGB evolutionary phase, which lasts of order  $10^7$  yr, are extremely complex, depending strongly on the (poorly known) mass loss rates, and the reader is referred to the quoted papers, and also to the recent monograph by [120] and reviews by [145, 129, 223], for more detailed descriptions of the physics and phenomenology surrounding AGB stars.

Once the AGB star's envelope mass has become very low, a final, quite dramatic mass ejection episode may take place, the so-called “superwind phase” ([208]), whose origin and nature still remain the subject of much debate. One way or another, the ejection of the outer layers of the AGB stars is expected to lead to the formation of a so-called “post-AGB star” (see Fig. 6), which is basically the bare core of the progenitor AGB star finally exposed. (Surrounding such a post-AGB star a planetary nebula may also be found, in which the ejected gas is being “lit up” by the central star.) Following a very quick evolution to the blue across the HRD, the star finally settles on the WD cooling sequence (Fig. 5). The latter, in fact, represents the “death bed” of a low-mass star, provided, of course, it does not somehow acquire mass from/merge with a companion – but that would be quite a different story.

Before closing, we note that a low-mass star may reach the WD cooling curve following other evolutionary routes, including the following: (i) Directly after the RGB, bypassing the HB and AGB phases, which may happen if somehow mass loss on the RGB is so extreme that the He core never gets to grow to the minimum level required for He ignition. In this case, a He WD is formed, not a C-O one. (ii) Directly after the HB, bypassing the AGB phase, which may happen if the star arrives on the ZAHB at a very high temperature (i.e., as an EHB or sdB star). This has been called the “AGB manquè” route ([115]). (iii) Directly from the (early) AGB phase, i.e., prior to the thermal pulsing phase. This so-called “post-early AGB” route ([26]) can take place also in the case of EHB or sdB stars, though for cooler ones than in the case of AGB manquè stars (see, e.g., [94]). Post-AGB, AGB manquè, and post-early AGB stars, when present, can be important contributors to the integrated ultraviolet light from old stellar populations (see, e.g., [80, 94, 92, 178, 181]).

## ACKNOWLEDGMENTS

I would like to thank the organizers for the invitation and for helping make our stay in Rio so pleasant. I am particularly indebted to A. V. Sweigart for providing some of the data (MS evolution and later) that was used in producing Figs. 5 and 6, and to him and R. T. Rood for several perceptive comments and useful suggestions. A critical reading of the manuscript by H. A. Smith and A. Valcarce is also gratefully acknowledged. Financial support was provided by the organizing committee and by Proyectos FONDECYT Regulares No. 1030954 and 1071002.

## REFERENCES

1. Alexander, D. R., & Ferguson, J. W. 1994, *ApJ*, 437, 879
2. Allende Prieto, C., Lambert, D. L., & Asplund, M. 2001, *ApJ*, 556, L63
3. Angulo, C., et al. 1999, *Nuc. Phys. A*, 656, 3
4. Asida, S. M. 2000, *ApJ*, 528, 896
5. Asplund, M. 2005, *ARA&A*, 43, 481
6. Asplund, M., Grevesse, N., Sauval, A. J., Allende Prieto, C., & Kiselman, D. 2004, *A&A*, 417, 751
7. Assunção, M., et al. 2006, *Phys. Rev. C*, 73, 055801
8. Badhnel, N. R., Bautista, M. A., Butler, K., Delahaye, F., Mendoza, C., Palmeri, P., Zeippen, C. J., & Seaton, M. J. 2005, *MNRAS*, 360, 458
9. Bahcall, J. N., & Pinsonneault, M. H. 1995, *Rev. Mod. Phys.*, 67, 781
10. Bahcall, J. N., Pinsonneault, M. H., & Basu, S. 2001, *ApJ*, 555, 990
11. Bahcall, J. N., Serenelli, A. M., & Basu, S. 2005, *ApJ*, 621, L85
12. Bascoul, G. P. 2006, in *Convection in Astrophysics*, IAU Symp. 239, ed. F. Kupka, I. W. Roxburgh, & K. L. Chan (Cambridge: Cambridge University), 71
13. Basu, S., Chaplin, W. J., Elsworth, Y., New, R., Serenelli, A. M., & Verner, G. A. 2007, *ApJ*, 655, 660
14. Bedin, L. R., Piotto, G., Anderson, J., Cassisi, S., King, I. R., Momany, Y., & Carraro, G. 2004, *ApJ*, 605, L125
15. Bekki, K., Campbell, S. W., Lattanzio, J. C., & Norris, J. E. 2007, *MNRAS*, in press (astro-ph/0702289)
16. Benvenuto, O. G., & De Vito, M. A. 2004, *MNRAS*, 352, 249
17. Bergbusch, P. A., & VandenBerg, D. A. 1992, *ApJS*, 81, 163
18. Bethe, H. A. 1939, *Phys. Rev.*, 55, 434

19. Bethe, H. A., & Marshak, R. E. 1939, *Rep. Prog. Phys.*, 6, 1
20. Biesiada, M., & Malec, B. 2002, *Phys. Rev. D*, 65, 043008
21. Bodenheimer, P. 1992, in *Star Formation in Stellar Systems*, ed. G. Tenorio-Tagle, M. Prieto, & F. Sánchez (Cambridge: Cambridge University), 3
22. Böhm-Vitense, E. 1958, *ZfA*, 46, 108
23. Böhm-Vitense, E. 2004, *AJ*, 128, 2435
24. Böhm-Vitense, E., Evans, N. R., Carpenter, K., Morgan, S., Beck-Winchatz, B., & Robinson, R. 1997, *AJ*, 114, 1176
25. Bressan, A., Bertelli, G., & Chiosi, C. 1986, *MmSAIt*, 57, 411
26. Brocato, E., Matteucci, F., Mazzitelli, I., & Tornambè, A. 1990, *ApJ*, 349, 458
27. Brown, T. M., Sweigart, A. V., Lanz, T., Landsman, W. B., & Hubeny, I. 2001, *ApJ*, 562, 368
28. Brunt, D. 1927, *Quart. J. Roy. Meteor. Soc.*, 53, 30
29. Buonanno, R., Corsi, C. E., & Fusi Pecci, F. 1985, *A&A*, 145, 97
30. Burbidge, E. M., Burbidge, G. R., Fowler, W. A., & Hoyle, F. 1957, *Rev. Mod. Phys.*, 29, 547
31. Burgasser, A. J., et al. 1999, *ApJ*, 522, L65
32. Cai, T. 2006, *Ch. Astr. Astrop.*, 30, 284
33. Caloi, V., & D'Antona, F. 2007, *A&A*, 463, 949
34. Caloi, V., & Mazzitelli, I. 1993, *A&A*, 271, 139
35. Cameron, A. G. W. 1957, *PASP*, 69, 201
36. Canuto, V. M. 1999, *ApJ*, 524, 311
37. Canuto, V. M. 2000a, *A&A*, 357, 177
38. Canuto, V. M. 2000b, *ApJ*, 534, L113
39. Canuto, V. M., Goldman, I., & Mazzitelli, I. 1996, *ApJ*, 473, 550
40. Canuto, V. M., & Mazzitelli, I. 1991, *ApJ*, 370, 295
41. Canuto, V. M., & Mazzitelli, I. 1992, *ApJ*, 389, 724
42. Caputo, F., Chieffi, A., Tornambè, A., Castellani, V., & Pulone, L. 1989, *ApJ*, 340, 241
43. Cassisi, S., Castellani, V., Degl'Innocenti, S., Piotto, G., & Salaris, M. 2001, *A&A*, 366, 578
44. Cassisi, S., Potekhin, A. Y., Pietrinferni, A., Catelan, M., & Salaris, M. 2007, *ApJ*, in press (astro-ph/0703011)
45. Cassisi, S., Salaris, M., & Bono, G. 2002, *ApJ*, 565, 1231
46. Cassisi, S., Salaris, M., Castelli, F., & Pietrinferni, A. 2004, *ApJ*, 616, 498
47. Cassisi, S., Schlattl, H., Salaris, M., & Weiss, A. 2003, *ApJ*, 582, L43
48. Castellani, M., & Castellani, V. 1993, *ApJ*, 407, 649
49. Castellani, M., Castellani, V., & Prada Moroni, P. G. 2006, *A&A*, 457, 569
50. Castellani, V., Chieffi, A., Tornambè, A., & Pulone, L. 1985, *ApJ*, 296, 204
51. Castellani, V., Giannone, P., & Renzini, A. 1971a, *Ap&SS*, 10, 340
52. Castellani, V., Giannone, P., & Renzini, A. 1971b, *Ap&SS*, 10, 355
53. Castellani, V., & Renzini, A. 1968, *Ap&SS*, 2, 310
54. Catelan, M. 2000, *ApJ*, 531, 826
55. Catelan, M. 2005, preprint (astro-ph/0507464)
56. Catelan, M., de Freitas Pacheco, J. A., & Horvath, J. E. 1996, *ApJ*, 461, 231
57. Cepa, J. 2004, *A&A*, 422, 831
58. Chabrier, G., & Baraffe, I. 2000, *ARA&A*, 38, 337
59. Chandrasekhar, S. 1939, *An Introduction to the Study of Stellar Structure* (Chicago: University of Chicago)
60. Charbonnel, C. 1995, *ApJ*, 453, L41
61. Charbonnel, C. 2005, in *Cosmic Abundances as Records of Stellar Evolution and Nucleosynthesis*, ASP Conf. Ser., Vol. 336, ed. T. G. Barnes III & F. N. Bash (San Francisco: ASP), 119
62. Charbonnel, C., & Balachandran, S. C. 2000, *A&A*, 359, 563
63. Charpinet, S., Fontaine, G., Brassard, P., & Dorman, B. 1996, *ApJ*, 471, L103
64. Chiappini, C., Romano, D., & Matteucci, F. 2003, *MNRAS*, 339, 63
65. Chieffi, A., Straniero, O., & Salaris, M. 1995, *ApJ*, 445, L39
66. Chiosi, C. 1999, in *Theory and Tests of Convection in Stellar Structure*, ASP Conf. Ser., Vol. 173, ed. A. Giménez, E. F. Guinan, & B. Montesinos (San Francisco: ASP), 9
67. Chiosi, C., Bertelli, G., & Bressan, A. 1992, *ARA&A*, 30, 235
68. Choi, E., & Yi, S. K. 2007, *MNRAS*, 375, L1

69. Chuzhoy, L. 2006, MNRAS, 369, L52

70. Claret, A. 2006, A&A, 453, 769

71. Clayton, D. D. 1968, Principles of Stellar Evolution and Nucleosynthesis (New York: McGraw-Hill)

72. Cook, C. W., Fowler, W. A., Lauritsen, C. C., & Lauritsen, T. 1957, Phys. Rev., 107, 508

73. Cox, A. N. 1991, ApJ, 381, L71

74. Cox, A. N. 1998, ApJ, 496, 246

75. Cox, J. P. 1976, ARA&A, 14, 247

76. Cox, J. P., & Giuli, R. T. 1968, Principles of Stellar Structure (New York: Gordon and Breach)

77. D'Antona, F., Bellazzini, M., Caloi, V., Fusi Pecci, F., Galleti, S., & Rood, R. T. 2005, ApJ, 631, 868

78. D'Cruz, N. L., Dorman, B., Rood, R. T., & O'Connell, R. W. 1996, ApJ, 466, 359

79. Dearborn, D. S. P., Lattanzio, J. C., & Eggleton, P. P. 2006, ApJ, 639, 405

80. de Boer, K. S. 1985, A&A, 142, 321

81. Degl'Innocenti, S., Prada Moroni, P. G., & Ricci, B. 2006, Ap&SS, 305, 67

82. de la Reza, R., Drake, N. A., da Silva, L., Torres, C. A. O., & Martin, E. L. 1997, ApJ, 482, L77

83. Demarque, P. R., & Larson, R. B. 1964, ApJ, 140, 544

84. Demarque, P., & Mengel, J. G. 1972, ApJ, 171, 583

85. De Medeiros, J. R., do Nascimento Jr., J. D., Sankarankutty, S., Costa, J. M., & Maia, M. R. G. 2000, A&A, 363, 239

86. Deng, L., Bressan, A., & Chiosi, C. 1996, A&A, 313, 145

87. Denissenkov, P. A., Chaboyer, B., & Li, K. 2006, ApJ, 641, 1087

88. Denissenkov, P. A., & Herwig, F. 2004, ApJ, 612, 1081

89. Denissenkov, P. A., & VandenBerg, D. A. 2003, ApJ, 593, 509

90. Dewitt, H. E., Grboske, H. C., & Cooper, M. S. 1973, ApJ, 181, 439

91. do Nascimento Jr., J. D., Canto Martins, B. L., Melo, C. H. F., Porto de Mello, G., & De Medeiros, J. R. 2003, A&A, 405, 723

92. Dorman, B., O'Connell, R. W., & Rood, R. T. 1995, ApJ, 442, 105

93. Dorman, B., & Rood, R. T. 1993, ApJ, 409, 387

94. Dorman, B., Rood, R. T., & O'Connell, R. W. 1993, ApJ, 419, 596

95. Dyer, P., & Barnes, C. A. 1974, Nucl. Phys. A, 233, 495

96. Eddington, A. S. 1926, The Internal Constitution of the Stars (Cambridge: Cambridge University Press)

97. Eggleton, P. P., Dearborn, D. S. P., & Lattanzio, J. C. 2006, Science, 314, 1580

98. Ferguson, J. W., Alexander, D. R., Allard, F., Barman, T., Bodnarik, J. G., Hauschildt, P. H., Heffner-Wong, A., & Tamanai, A. 2005, ApJ, 623, 585

99. Ferraro, F. R., Valenti, E., Straniero, O., & Origlia, L. 2006, ApJ, 642, 225

100. França, U., & Rosenfeld, R. 2004, Phys. Rev. D, 69, 063517

101. Freytag, S., & Salaris, M. 1999, ApJ, 513, L49

102. Fukugita, M., Hogan, C. J., & Peebles, P. J. E. 1998, ApJ, 503, 518

103. Fusi Pecci, F., Ferraro, F. R., Crocker, D. A., Rood, R. T., & Buonanno, R. 1990, A&A, 238, 95

104. Gallart, C. 1998, ApJ, 495, L43

105. Gamow, G. 1939, Phys. Rev., 55, 718

106. Gautschy, A., & Saio, H. 1995, ARA&A, 33, 75

107. Gingold, R. A. 1974, ApJ, 193, 177

108. Gingold, R. A. 1976, ApJ, 204, 116

109. Girardi, L. 1999, MNRAS, 308, 818

110. Gnedin, O. Y., Lahav, O., & Rees, M. J. 2001, preprint (astro-ph/0108034)

111. Grboske, H. C., Dewitt, H. E., Grossman, A. S., & Cooper, M. S. 1973, ApJ, 181, 457

112. Gratton, R. G., Sneden, C., Carretta, E. 2004, ARA&A, 42, 385

113. Gratton, R. G., Sneden, C., Carretta, E., & Bragaglia, A. 2000, A&A, 354, 169

114. Gray, D. F. 2005, The Observation and Analysis of Stellar Photospheres, Third Edition (Cambridge: Cambridge University)

115. Greggio, L., & Renzini, A. 1990, ApJ, 364, 35

116. Grevesse, N., & Sauval, A. J. 1998, Sp. Sc. Rev., 85, 161

117. Grundahl, F., VandenBerg, D. A., Bell, R. A., Andersen, M. I., & Stetson, P. B. 2000, AJ, 120, 1884

118. Guinan, E. F., & Ribas, I. 2002, in The Evolving Sun and its Influence on Planetary Environments, ASP Conf. Ser., Vol. 269, ed. B. Montesinos, A. Giménez, & E. F. Guinan (San Francisco: ASP), 85

119. Guzik, J. A., Watson, L. S., & Cox, A. N. 2006, MSAIt, 77, 389

120. Habing, H. J., & Olofsson, H. 2004, Asymptotic Giant Branch Stars (Heidelberg: Springer)

121. Haft, M., Raffelt, G., & Weiss, A. 1994, ApJ, 425, 222; erratum: 1995, ApJ, 438, 1017

122. Hannestad, S., & Raffelt, G. G. 2002, Phys. Rev. Letters, 88, 071301-1

123. Hansen, C. J., Kawaler, S. D., & Trimble, V. 2004, Stellar Interiors: Physical Principles, Structure, and Evolution (New York: Springer)

124. Härm, R., & Schwarzschild, M. 1966, ApJ, 145, 496

125. Hata, N., Scherrer, R. J., Steigman, G., Thomas, D., Walker, T. P., & Bludman, S. 1995, Phys. Rev. Lett., 75, 3977

126. Hayashi, C. 1966, ARA&A, 4, 171

127. Henyey, L. G., Forbes, J. E., & Gould, N. L. 1964, ApJ, 139, 306

128. Henyey, L., Vardya, M. S., & Bodenheimer, P. 1965, ApJ, 142, 841

129. Herwig, F. 2005, ARA&A, 43, 435

130. Hollowell, D., & Iben, I., Jr. 1989, ApJ, 340, 966

131. Hoyle, F., Dunbar, D. N. F., Wenzel, W. A., & Whaling, W. 1953, Phys. Rev., 92, 1095

132. Hoyle, F., Fowler, W. A., Burbidge, G. R., & Burbidge, E. M. 1956, Science, 124, 611

133. Hubbard, W. B., & Lampe, M. 1969, ApJS, 18, 297

134. Iben, I., Jr. 1964, ApJ, 140, 1631

135. Iben, I., Jr. 1965, ApJ, 141, 993; erratum: 1965, ApJ, 142, 421

136. Iben, I., Jr. 1967a, ApJ, 147, 624

137. Iben, I., Jr. 1967b, ApJ, 147, 650

138. Iben, I., Jr. 1968a, ApJ, 154, 581

139. Iben, I., Jr. 1968b, Nature, 220, 143

140. Iben, I., Jr. 1971, PASP, 83, 697

141. Iben, I., Jr. 1982, ApJ, 260, 821

142. Iben, I., Jr. 1991, ApJS, 76, 55

143. Iben, I., Jr., & Renzini, A. 1982a, ApJ, 259, L79

144. Iben, I., Jr., & Renzini, A. 1982b, ApJ, 263, L23

145. Iben, I., Jr., & Renzini, A. 1983, ARA&A, 21, 271

146. Iben, I., Jr., & Rood, R. T. 1970, ApJ, 161, 587

147. Iglesias, C. A., & Rogers, F. J. 1996, ApJ, 464, 943

148. Itoh, N., Hayashi, H., Nishikawa, A., & Kohyama, Y. 1996, ApJS, 102, 411

149. Itoh, N., Mitake, S., Iyetomi, H., & Ichimaru, S. 1983, ApJ, 273, 774

150. Jeans, J. H. 1902, Phil. Trans. A, 199, 1

151. Jeffery, C. S., & Saio, H. 2006, MNRAS, 372, L48

152. Karakas, A. I., Fenner, Y., Sills, A., Campbell, S. W., & Lattanzio, J. C. 2006, ApJ, 652, 1240

153. Kato, S. 1966, PASJ, 18, 374

154. King, C. R., Da Costa, G. S., & Demarque, P. 1985, ApJ, 299, 674

155. Kippenhahn, R., Weigert, A., & Hofmeister, E. 1967, in Methods in Computational Physics, Vol. 7, ed. B. Alder, S. Fernbach, & M. Rotenberg (New York: Academic Press), 129

156. Kirkpatrick, J. D., et al. 1999, ApJ, 519, 802

157. Krauss, L. M. 2003, ApJ, 596, L1

158. Krauss, L. M. 2004, ApJ, 604, 481

159. Krauss, L. M., & Chaboyer, B. 2003, Science, 299, 65

160. Kravtsov, A. V., & Gnedin, O. Y. 2005, ApJ, 623, 650

161. Kremer, R. M., Barnes, C. A., Chang, K. H., Evans, H. C., Filippone, B. W., Hahn, K. H., & Mitchell, L. W. 1988, Phys. Rev. Lett., 60, 1475

162. Krishna Swamy, K. S. 1966, ApJ, 145, 174

163. Kroupa, P. 2002, Science, 295, 82

164. Kunz, R., Fey, M., Jaeger, M., Mayer, A., Hammer, J. W., Staudt, G., Harissopoulos, S., & Paradellis, T. 2002, ApJ, 567, 643

165. Kunz, R., Jaeger, M., Mayer, A., Hammer, J. W., Staudt, G., Harissopoulos, S., & Paradellis, T. 2001, Phys. Rev. Lett., 86, 3244

166. Lanz, T., Brown, T. M., Sweigart, A. V., Hubeny, I., & Landsman, W. B. 2004, ApJ, 602, 342

167. Ledoux, P. 1947, ApJ, 105, 305

168. Ledoux, P., & Walraven, Th. 1958, Hanbduch der Physik, 51, 353

169. Lee, Y.-W., et al. 2005, *ApJ*, 621, L57

170. Ludwig, H.-G., Freytag, B., & Steffen, M. 1999, *A&A*, 346, 111

171. Meakin, C. A., & Arnett, D. 2007, *ApJ*, submitted (astro-ph/0611315)

172. Meissner, F., & Weiss, A. 2006, *A&A*, 456, 1085

173. Mengel, J., & Sweigart, A. V. 1981, in IAU Colloq. 68, *Astrophysical Parameters for Globular Clusters*, ed. A. G. D. Philip & D. S. Hayes (Schenectady: L. Davis), 277

174. Metcalfe, T. S. 2003, *ApJ*, 587, L43

175. Merryfield, W. J. 1995, *ApJ*, 444, 318

176. Miglio, A., Montalbán, J., & Dupret, M.-A. 2007, *MNRAS*, 375, L21

177. Moehler, S. 2001, *PASP*, 113, 1162

178. Moehler, S., Landsman, W., & Napiwotzki, R. 1998, *A&A*, 335, 510

179. Naur, P., & Ostebrock, D. 1953, *ApJ*, 117, 306

180. Norris, J. E. 2004, *ApJ*, 612, L25

181. O'Connell, R. W. 1999, *ARA&A*, 37, 603

182. Olive, K. A., Rood, R. T., Schramm, D. N., Truran, J., & Vangioni-Flam, E. 1995, *ApJ*, 444, 680

183. Öpik, E. J. 1951, *Proc. Roy. Irish Acad. A*, 54, 49

184. Ouellet, J. M. L., et al. 1992, *Phys. Rev. Lett.*, 69, 1896

185. Paczyński, B. 1969, *AcA*, 19, 1

186. Palacios, A., Charbonnel, C., Talon, S., & Siess, L. 2006, *A&A*, 453, 261

187. Palmieri, R., Piotto, G., Saviane, I., Girardi, L., & Castellani, V. 2002, *A&A*, 392, 115

188. Paparó, M., Szeidl, B., Saad, S. M., Kolláth, Z., & Abu Elazm, M. S. 2002, *A&A*, 391, 633

189. Piersanti, L., Straniero, O., & Cristallo, S. 2007, *A&A*, 462, 1051

190. Pietrinferni, A., Cassisi, S., Salaris, M., & Castelli, F. 2004, *ApJ*, 612, 168

191. Piotto, G., et al. 2005, *ApJ*, 621, 777

192. Potekhin, A. Y. 1999, *A&A*, 351, 787

193. Potekhin, A. Y., Baiko, D. A., Haensel, P., & Yakovlev, D. G. 1999, *A&A*, 346, 345

194. Pritzl, B. J., Venn, K. A., & Irwin, M. 2005, *AJ*, 130, 2140

195. Pulone, L. 1992, *MmSAIt*, 63, 485

196. Raffelt, G. G. 1990, *ApJ*, 365, 559

197. Raffelt, G. G. 1996, *Stars as Laboratories for Fundamental Physics: The Astrophysics of Neutrinos, Axions, and other Weakly Interacting Particles* (Chicago: University of Chicago)

198. Raffelt, G. G. 1999, *Phys. Rep.*, 320, 319

199. Raffelt, G. G. 2000, *Phys. Rep.*, 333-334, 593

200. Raffelt, G. G. 2003, in *Astronomy, Cosmology and Fundamental Physics*, ed. P. A. Shaver, L. DiLella, & A. Giménez (Berlin: Springer-Verlag), p. 334

201. Raffelt, G. G. 2007a, preprint (hep-ph/0611118)

202. Raffelt, G. G. 2007b, preprint (hep-ph/0611350)

203. Raffelt, G. G., & Dearborn, D. S. P. 1987, *Phys. Rev. D*, 36, 2211

204. Raffelt, G. G., & Weiss, A. 1992, *A&A*, 264, 536

205. Rampino, M. R., & Caldeira, K. 1994, *ARA&A*, 32, 83

206. Recio-Blanco, A., & de Laverny, P. 2007, *A&A*, 461, L13

207. Redder, A., Becker, H. W., Rolfs, C., Trautvetter, H. P., Donoghue, T. R., Rinckel, T. C., Hammer, J. W., & Langanke, K. 1987, *Nucl. Phys. A*, 462, 385

208. Renzini, A. 1981, in *Effects of Mass Loss on Stellar Evolution*, ed. C. Chiosi & R. Stalio (Dordrecht: Reidel), 319

209. Renzini, A. 1987, *A&A*, 188, 49

210. Renzini, A. 2006, *ARA&A*, 44, 141

211. Renzini, A., & Fusi Pecci, F. 1988, *ARA&A*, 26, 199

212. Robertson, J. W., & Faulkner, D. J. 1972, *ApJ*, 171, 309

213. Rogers, F. J., & Iglesias, C. A. 2000, *Sp. Sc. Rev.*, 85, 61

214. Rolfs, C. E., & Rodney, W. S. 1988, *Cauldrons in the Cosmos* (Chicago: University of Chicago)

215. Romano, D., Matteucci, F., Tosi, M., Pancino, E., Bellazzini, M., Ferraro, F. R., Limongi, M., & Sollima, A. 2007, *MNRAS*, 376, 405

216. Rood, R. T. 1972, *ApJ*, 177, 681

217. Rood, R. T. 1973, *ApJ*, 184, 815

218. Roters, G., Rolfs, C., Strieder, F., & Trautvetter, H. P. 1999, *Eur. Phys. J. A*, 6, 451

219. Roxburgh, I. W. 1965, MNRAS, 130, 223

220. Roxburgh, I. W. 1978, A&A, 65, 281

221. Roxburgh, I. W. 1989, A&A, 211, 361

222. Sackmann, I.-J., Boothroyd, A. I., & Kraemer, K. E. 1993, ApJ, 418, 457

223. Salaris, M., & Cassisi, S. 2005, Evolution of Stars and Stellar Populations (Chichester: Wiley)

224. Salaris, M., Cassisi, S., & Weiss, A. 2002, PASP, 114, 375

225. Salaris, M., Chieffi, A., & Straniero, O. 1993, ApJ, 414, 580

226. Salpeter, E. E. 1952, ApJ, 115, 326

227. Salpeter, E. E. 1955, ApJ, 121, 161

228. Salpeter, E. E. 2002, ARA&A, 40, 1

229. Sandage, A. R. 1953, AJ, 58, 61

230. Sarajedini, A., et al. 2007, AJ, 133, 1658

231. Schönberg, M., & Chandrasekhar, S. 1942, ApJ, 96, 161

232. Schönberner, D. 1979, A&A, 79, 108

233. Schwarzschild, K. 1906, Gött. Nachr., 1, 41

234. Schwarzschild, M. 1958, Structure and Evolution of the Stars (Princeton: Princeton University Press)

235. Schwarzschild, M., & Härm, R. 1958, ApJ, 128, 348

236. Schwarzschild, M., & Härm, R. 1962, ApJ, 136, 158

237. Schwarzschild, M., & Härm, R. 1965, ApJ, 142, 855

238. Schwarzschild, M., & Härm, R. 1970, ApJ, 160, 341

239. Schwarzschild, M., & Selberg, H. 1962, ApJ, 136, 150

240. Seaton, M. 2005, MNRAS, 362, L1

241. Seaton, M. J., & Badnell, N. R. 2004, MNRAS, 354, 457

242. Serenelli, A., & Weiss, A. 2005, A&A, 442, 1041

243. Shi, X. 1995, ApJ, 446, 637

244. Shternin, P. S., & Yakovlev, D. G. 2006, Phys. Rev. D, 74, 043004

245. Sills, A., & Pinsonneault, M. H. 2000, ApJ, 540, 489

246. Simon, N. R. 1995, in Astrophysical Applications of Powerful New Databases, ASP Conf. Ser., Vol. 78, ed. S. J. Adelman & W. L. Wiese (San Francisco: ASP), 211

247. Simon, N. R., & Kanbur, S. M. 1992, RMxAA, 23, 253

248. Spergel, D. N., et al. 2003, ApJS, 148, 175

249. Spergel, D. N., et al. 2007, ApJ, in press (astro-ph/0603449)

250. Spiegel, E. A. 1971, ARA&A, 9, 323

251. Stix, M. 2002, The Sun, Second Edition (Berlin: Springer)

252. Straniero, O., Gallino, R., & Cristallo, S. 2006, Nucl. Phys. A, 777, 311

253. Sweigart, A. V. 1990, in Confrontation between Stellar Pulsation and Evolution, ASP Conf. Ser., Vol. 11, ed. C. Cacciari & G. Clementini (San Francisco: ASP), 1

254. Sweigart, A. V. 1994a, ApJ, 426, 612

255. Sweigart, A. V. 1994b, in Hot Stars in the Galactic Halo, ed. S. J. Adelman, C. R. Upgren, & C. J. Adelman (Cambridge: Cambridge University), 17

256. Sweigart, A. V., & Demarque, P. 1972, ApJ, 171, 583

257. Sweigart, A. V., & Demarque, P. 1973, in Variable Stars in Globular Clusters, ed. J. D. Fernie (Dordrecht: Reidel), 221

258. Sweigart, A. V., Gregg, L., & Renzini, A. 1989, ApJS, 69, 911

259. Sweigart, A. V., Gregg, L., & Renzini, A. 1990, ApJ, 364, 527

260. Sweigart, A. V., & Gross, P. G. 1974, ApJS, 32, 367

261. Sweigart, A. V., & Gross, P. G. 1976, ApJ, 190, 101

262. Sweigart, A. V., & Gross, P. G. 1978, ApJS, 36, 405

263. Sweigart, A. V., & Mengel, J. G. 1979, ApJ, 229, 624

264. Sweigart, A. V., & Renzini, A. 1979, A&A, 71, 66

265. Swihart, T. L. 1972, Physics of Stellar Interiors (Tucson: Pachart)

266. Tayler, R. 1952, MNRAS, 112, 387

267. Thomas, H.-C. 1967, ZfA, 67, 420

268. Tsytovich, V. N., Bingham, R., de Angelis, U., & Forlani, A. 1996, Phys. Scripta, 54, 312

269. Tsytovich, V. N., Bingham, R., de Angelis, U., & Forlani, A. 2001, J. Quant. Spectr. Rad. Transfer, 69, 9

270. Väisälä, V. 1925, *Soc. Sci. Fennica, Comm. Phys. Mat.* II, 2, 46

271. VandenBerg, D. A. 1992, *ApJ*, 391, 685

272. VandenBerg, D. A., Bergbusch, P. A., & Dowler, P. D. 2006, *ApJS*, 162, 375

273. VandenBerg, D. A., Richard, O., Michaud, G., & Richer, J. 2002, *ApJ*, 571, 487

274. VandenBerg, D. A., Swenson, F. J., Rogers, F. J., Iglesias, C. A., & Alexander, D. R. 2000, *ApJ*, 532, 430

275. Ventura, P., & D'Antona, F. 2006, *A&A*, 457, 995

276. Villanova, S., et al. 2007, *ApJ*, in press (astro-ph/0703208)

277. Vink, J. S., & Cassisi, S. 2002, *A&A*, 392, 553

278. Vitense, E. 1953, *ZfA*, 32, 135

279. Weiss, A., Salaris, M., Ferguson, J. W., & Alexander, D. R. 2007, *A&A*, in press (astro-ph/0605666)

280. Weiss, A., Serenelli, A., Kitsikis, A., Schlattl, H., & Christensen-Dalsgaard, J. 2005, *A&A*, 441, 1129

281. Wheeler, J. C., Sneden, C., & Truran, J. W., Jr. 1989, *ARA&A*, 27, 279

282. Wuchterl, G., & Klessen, R. S. 2001, *ApJ*, 560, L185

283. Yakovlev, D. G., & Shalybkov, D. A. 1989, *Astrophys. Space Phys. Rev. (Sov. Sci. Rev. E)*, 7, 311

284. Zahn, J.-P. 1992, *A&A*, 265, 115

285. Ziman, J. M. 1960, *Electrons and Phonons* (Oxford: Oxford University)

286. Zoccali, M., et al. 2006, *A&A*, 457, L1